Title: Elevation-based probabilistic mapping of irregularly flooded wetlands along the northern Gulf of Mexico coast

Authors: Nicholas M. Enwright[1], Wyatt C. Cheney[2], Kristine O. Evans[3], Hana R. Thurman[4], Mark S. Woodrey[5], Auriel M.V. Fournier[6], Dean B. Gesch[7], Jonathan L. Pitchford[8], Jason M. Stoker[9], and Stephen C. Medeiros[10]

Affiliations: [1]U.S. Geological Survey, Wetland and Aquatic Research Center, 700 Cajundome Boulevard, Lafayette, LA 70506, USA;

[2]Cheney Consulting under contract to the U.S. Geological Survey, Wetland and Aquatic Research Center, 700 Cajundome Boulevard, Lafayette, LA 70506, USA;

[3]Quantitative Ecology and Spatial Technologies (QuEST) Lab, Department of Wildlife, Fisheries and Aquaculture, Mississippi State University; Box 9690, Mississippi State, MS 39762, USA;

[4]Cherokee Nation System Solutions, under contract to the U.S. Geological Survey, Wetland and Aquatic Research Center, 700 Cajundome Boulevard, Lafayette, LA 70506, USA;

[5]Department of Wildlife, Fisheries and Aquaculture & Coastal Research and Extension Center, Mississippi State University, 1815 Popps Ferry Road, Biloxi, MS 39532, USA;

[6]Forbes Biological Station–Bellrose Waterfowl Research Center, Illinois Natural History Survey, Prairie Research Institute, University of Illinois at Urbana-Champaign, 20003 N CR 1770E, Havana, IL 62644, USA;

[7]U.S. Geological Survey, Earth Resources Observation and Science Center, 47914 252nd Street, Sioux Falls, SD 57198, USA;

[8]Grand Bay National Estuarine Research Reserve, 6005 Bayou Heron Rd. Moss Point, MS 39562, USA;

[9]U.S. Geological Survey, National Geospatial Program, 2150 Centre Ave, Building C, Fort Collins, CO 80526, USA;

[10]Embry-Riddle Aeronautical University, Department of Civil Engineering, 1 Aerospace Blvd, Daytona Beach, FL 32779, USA;

Corresponding author: Nicholas M. Enwright, U.S. Geological Survey, Wetland and Aquatic Research Center, Lafayette, LA 70506, USA; enwrightn@usgs.gov; 337-262-7613

Abstract

Irregularly flooded wetlands are found above the mean high water tidal datum and are exposed to tides and saltwater less frequently than daily. These wetlands provide important ecosystem services, such as providing habitat for fish and wildlife, enhancing water quality, ameliorating flooding impacts, supporting coastal food webs, and protecting upslope areas from erosion. Mapping irregularly flooded wetlands is challenging given their expansive coverage and dynamic nature. Furthermore, coastal wetlands are expected to change over the coming century due to sea-level rise and changes in the frequency and intensity of extreme storms. Consequently, coastal managers need baseline information on the spatial distribution of wetlands along with efficient and repeatable methods for observing changes. In this study, we used coastal wetlands from existing land use land cover data, best available lidar-derived digital elevation models, and Monte Carlo simulations to incorporate elevation uncertainty to create a probabilistic map of irregularly flooded wetlands along the northern Gulf of Mexico coast (USA). Our approach integrated findings from a review of coastal wetland elevation error in lidar datasets and an analysis of spatial autocorrelations of wetland elevation. We found a positive correlation ($r = 0.563$, $p < 0.0001$) when comparing the probability estimated from a digital elevation model and in situ elevation observations. The differences in probability had a mean bias error of -0.04 (i.e., digital elevation model-based probability tends to be slightly lower), a mean absolute error of 0.20, and a root mean square error of 0.26. Beyond this overall validation, we explored error metrics for land cover classes and lidar collection details. To quantify areal coverage of the probabilistic output, we classified the probability values into equal bins using an interval of 0.33. The areal coverage of the lowest probability bin ("unlikely"; probability ≤ 0.33) was separated into the upper and lower portions of the irregularly flooded wetland zone. Of the coastal wetlands along the northern Gulf of Mexico coast about 38% were classified as unlikely and low with the greatest coverage in south Louisiana and the Everglades and around 33%

were classified as unlikely and high with the greatest coverage in the Everglades and Texas. The relative coverage within the highest probability bin ("likely"; probability > 0.66) covered around 13%, with the greatest coverage in south Florida, south Louisiana, and Texas. The framework developed in this study can be transferred to other coastal wetland areas and updated to observe changes with sea-level rise.

Highlights

- Produced a probabilistic map of irregularly flooded wetlands.
- Included sources of uncertainty and wetland elevation spatial autocorrelation.
- Probability from digital elevation data generally agreed with in situ observations.
- Approach provides regional baseline and can be transferred to other areas.

Keywords

coastal wetlands, elevation uncertainty, lidar, Monte Carlo simulations, spatial autocorrelation

1. Introduction

Coastal wetlands are dynamic ecosystems that have adapted to changing sea level and climate throughout history (Jennerjahn et al., 2017; Saintilan et al., 2022). These wetlands provide habitat to numerous endemic species (Greenberg et al., 2006) along with many other valuable ecosystem services (Barbier et al., 2011). These systems are expected to experience widespread change in the future due to climate change and sea-level rise (Osland et al., 2022; Saintilan et al., 2022). To better manage coastal environments, coastal managers need baseline information on the current spatial distribution of wetlands and efficient and repeatable methods for observing change over time from climate change and sea-level rise.

Currently, there are several extensive mapping efforts in the United States that include coastal wetland information. These include the U.S. Fish and Wildlife Services' National Wetlands Inventory (U.S. Fish and Wildlife Service, 2022), the U.S. Geological Survey's (USGS) National Land Cover Database

(NLCD), USGS' Land Change Monitoring, Assessment, and Projection (LCMAP; Brown et al., 2020), and National Oceanic and Atmospheric Administration's (NOAA) Coastal Change Assessment Program (C-CAP; NOAA, 2016). a provide valuable information on the distribution and coverage of general cover types, researchers and land managers often require additional, more detailed wetland information on coastal vegetation zones based on salinity (Enwright et al., 2015) or need the development or refinement of products with a focus on tidal wetland inundation (O'Connell et al., 2017; Enwright et al., 2018; Holmquist et al., 2018; Brophy et al., 2019; Lamb et al., 2019; Holmquist and Windham-Myers, 2022; Narron et al., 2022).

Irregularly flooded wetlands are found above the mean high water tidal datum and are exposed to tides and saltwater less frequently than daily. In addition to typical tides, perigean spring tides, wind-induced water level fluctuations, and storms can play a major role in regulating flooding and salinity in coastal wetlands, especially in microtidal areas with frequent extreme storms, such as the northern Gulf of Mexico (USA; Stout, 1984). Maps with coastal wetland zonation based on salinity, such as those produced by Enwright et al. (2015), can be helpful because irregularly flooded wetlands can span a wide zone and are often mapped as palustrine wetlands in existing National Wetland Inventory or C-CAP maps, especially along the palustrine and estuarine ecotone. Evident from the palustrine and estuarine definitions, exposure to saline water is an important abiotic factor regulating coastal wetland zonation. Identifying these wetlands, which include supratidal areas, requires use of a water level that is higher than a tidal datum. For example, Brophy et al. (2019) developed a model to delineate the upper boundary of estuaries along the West Coast of the United States using elevation data and NOAA's 50% exceedance values for extreme water levels (e.g., Zervas et al., 2013). A similar approach could make use of NOAA's high-tide flooding levels (Sweet et al., 2018), which include inundation associated with perigean spring tides, wind-induced water level fluctuations, and storms. Land managers need observations of irregularly flooded wetlands because the frequency of contemporary high-tide flooding levels is expected to increase over the next several decades with accelerated sea-level rise (Sweet et al. 2018), and this increase is expected to have a high magnitude along the northern Gulf of Mexico in the 2030s (Thompson et al.,

2021). In addition to sea-level rise, the magnitude and intensity of extreme storms have been predicted to increase in the future with climate change (Knutson et al. 2010).

Delineating areas under a specific water level requires addressing multiple sources of elevation uncertainty including general uncertainty in elevation data (ASPRS, 2015), elevation error in coastal wetlands (Su and Bork, 2006; Schmid et al., 2011; Medeiros et al., 2015; Buffington et al., 2016; Medeiros et al., 2022), and for coastal areas, vertical datum transformation (Tang et al., 2018). Statistical models can be developed to reduce error in elevation data in coastal wetlands (Medeiros et al., 2015; Buffington et al., 2016; Cooper et al., 2019; Medeiros et al., 2022). While elevation data correction is optimal, in situ data availability issues can limit the ability to utilize this approach for spatially extensive regional studies. While accounting for lidar error, tidal datum uncertainty, and random uncertainty, Holmquist and Windham-Myers (2022) calculated relative tidal elevation for the conterminous United States using partial derivatives. This product normalizes elevation to tidal amplitude at MHW. Their layer was constrained to estuarine wetlands or adjacent palustrine wetlands that had a greater than 1% probability of being below an estimated mean higher high water spring (MHHWS) tide elevation layer (Holmquist et al., 2018) and any wetlands mapped as tidal in the National Wetland Inventory. In addition to relative tidal elevation, the study also included the development of a map of the probability of a wetland having an elevation below the MHW tidal datum (i.e., low marsh).

Monte Carlo simulations can be used to propagate these sources of uncertainty while also incorporating actual or assumed spatial autocorrelation of error using spatially explicit random fields (Wechsler and Kroll, 2006). This approach has been used to map intertidal areas (Enwright et al., 2018) and is commonly used for sea-level rise inundation (Cooper et al., 2013; Gesch 2018; Kulp and Strauss, 2019). In particular, Monte Carlo simulations may offer an alternative when statistical DEM correction is not feasible due to a regional study extent and limited in situ elevation data availability.

As previously mentioned, the delineation of irregularly flooded wetlands along microtidal coasts with frequent storms and wind-driven events may require the use of a water level that exceeds tidal datums alone. The objective of this study was to build on the work of Enwright et al. (2018) and Holmquist and

Windham-Meyers (2022) to develop probabilistic maps for irregularly flooded wetlands along the northern Gulf of Mexico. The research questions for this study are: (1) How can elevation data and uncertainty information for wetland elevation, tidal datums, and high-tide flooding be used to map the probability of irregularly flooded wetlands (i.e., the probability that an area is an irregularly flooded wetland based on elevation)?; (2) How can spatial autocorrelation be integrated into the probabilistic mapping?; (3) How does this map compare to probability from in situ elevation observations?; and (4) How does irregularly flooded wetland coverage vary across the Gulf of Mexico?

2. Methods

2.1. Study area

The study area was the northern Gulf of Mexico, which included five states — Texas, Louisiana, Mississippi, Alabama, and Florida (Fig. 1). Due to the gently sloping topography of the coastal plain, the region includes a substantial portion of the coastal wetlands in the conterminous USA (Greenberg et al., 2006). The northern Gulf of Mexico is a microtidal system with a tidal amplitude from 0.5–1 m (NOAA, 2019c) and a high proportion of brackish wetlands (Greenberg et al., 2006). Coastal wetland zonation and species composition vary along the northern Gulf of Mexico due to differences in geomorphology, climate, and management of coastal lands (Gabler et al., 2017). For example, south Texas has expansive tidal flats due to hypersaline conditions from arid conditions (Osland et al., 2013). Additionally, due to less frequent severe freezes, scrub/shrub and forested wetlands dominated by mangroves can be found in south Texas, the mid-coast of Texas, southeastern Louisiana, and south Florida, whereas coastal wetlands in other areas are often dominated by graminoid or succulent vegetation (Gabler et al., 2017). Regarding coastal wetland zonation and coverage, south Louisiana and south Florida have expansive coastal wetlands due to a low slope and spatially extensive low-lying lands (Reyer et al., 1988; Osland et al., 2022).

Consequently, data processing was conducted at the watershed-level for subregions along the northern Gulf of Mexico (Fig. 1). We used estuarine drainage areas delineated by Dale et al. (2022) as watershed boundaries. These watersheds were combined to form subregions along the northern Gulf of Mexico, which included: (1) Laguna Madre; (2) Texas Mid-Coast; (3) Chenier Plain; (4) Mid-Deltaic Plain; (5) Deltaic Plain; (6) Mississippi Sound; (7) Florida Panhandle; (8) Florida Big Bend; (9) West Peninsula Florida; (10) Everglades; and (11) Florida Keys (Fig. 1).

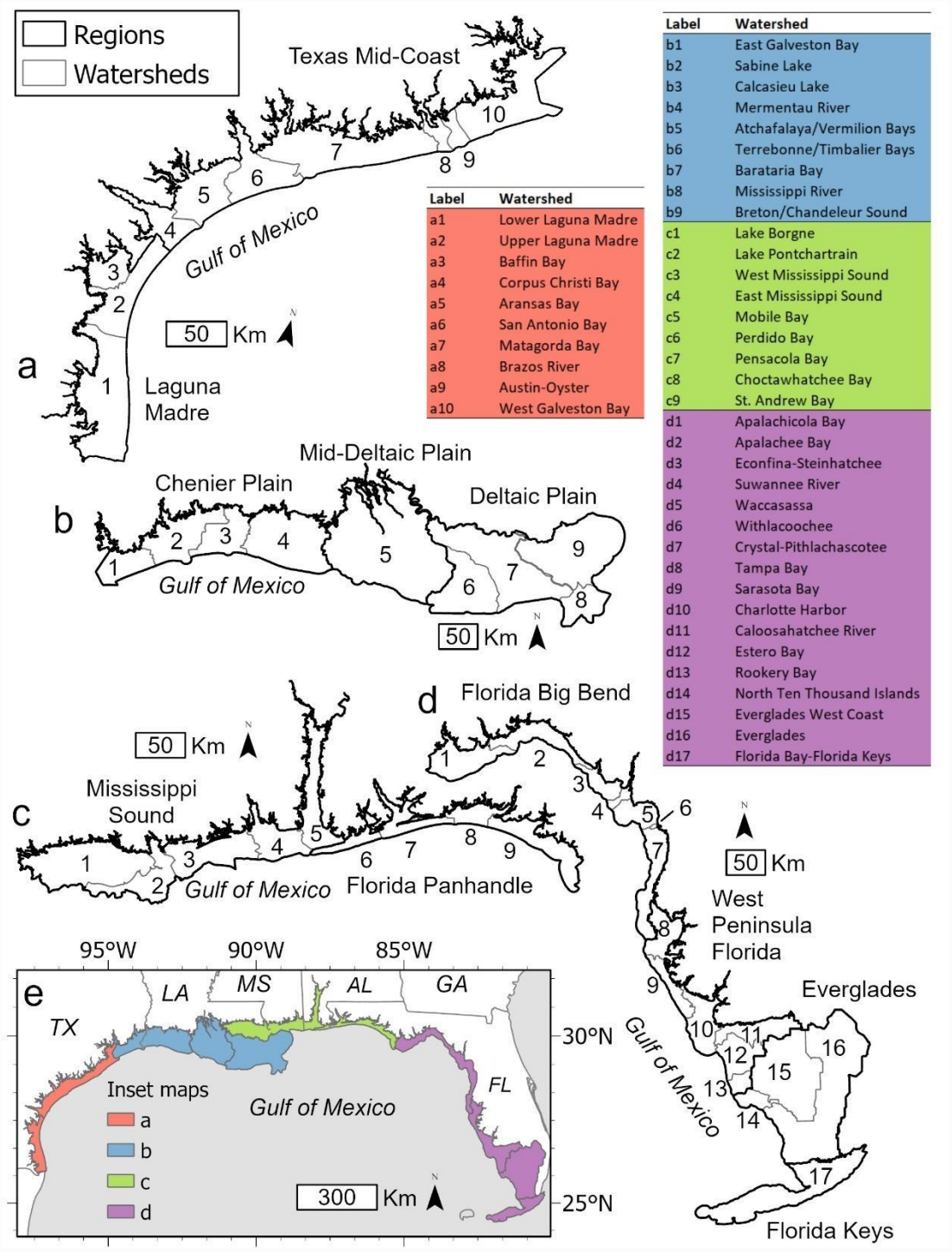

Fig. 1. Study area for mapping irregularly flooded wetland probability along the northern Gulf of Mexico coast, USA. **a-d** includes watersheds for groups of regions and **e** provides an overview of the study area. Watershed names are listed by inset map and number.

2.2. Coastal wetland mask

Existing land cover data and elevation data were used to constrain the study area to coastal wetlands. Specifically, the study area included coastal wetlands that fell within a generalized 5-m contour (relative to the North American Vertical Datum of 1988 [NAVD88]) that was created from 1/3 arc-second seamless DEMs (10 m) from the USGS 3D Elevation Program (3DEP) (USGS, 2020). We used land cover to develop a coastal wetland mask from NOAA's 2016 C-CAP 30-m dataset (NOAA, 2016) and 10-m C-CAP BETA land cover dataset (NOAA, 2019a). The coastal wetland mask included all estuarine emergent marsh, estuarine scrub/shrub wetlands, and estuarine forested wetlands. The coastal wetland mask also included adjacent wetlands that were connected to estuarine wetlands using 8-pixel connectivity (i.e., connectivity that can occur through cells in both cardinal and diagonal directions). Unless noted otherwise, the spatial data analysis was conducted using Esri ArcGIS Pro 2.9 (Redlands, California, USA). More details on the coastal wetland mask are included in Appendix A.

2.3. Mapping irregularly flooded wetland probability

The main objective of this study was to delineate irregularly flooded wetlands along the northern Gulf of Mexico coast. Figure 2 shows an overview of the process used for developing this product. The sections below cover the general methods used for this study. Additional details on the methods can be found in Appendix A.

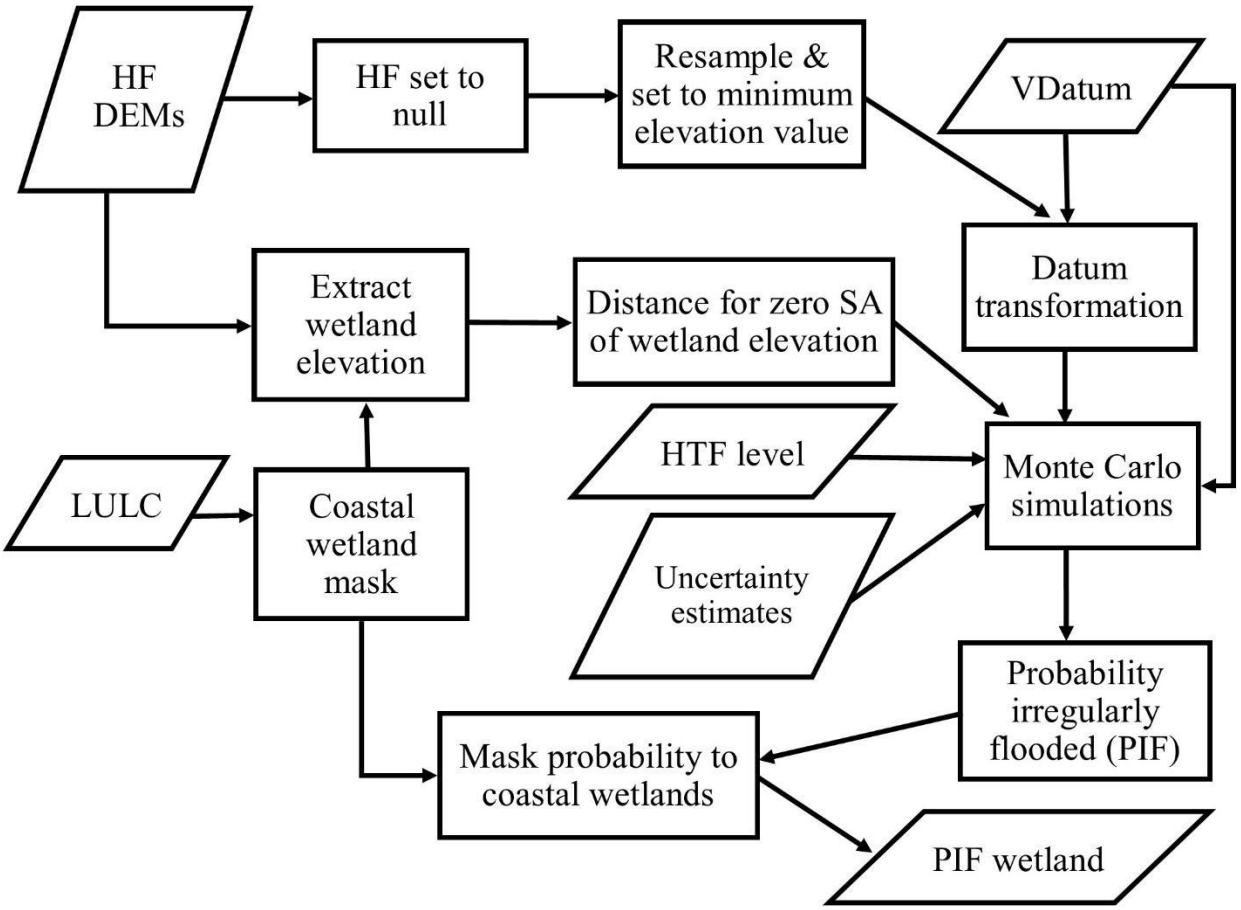

Fig. 2. An overview of the approach used for estimating the probability of an area being an irregularly flooded wetland along the northern Gulf of Mexico coast, USA. Uncertainty estimates included uncertainty from NOAA's high-tide flooding level (HTF; Sweet et al., 2018), coastal wetland elevation, and tidal datum transformation. HF, hydroflattened; DEMs, digital elevation models; LULC, land use land cover data; and VDatum, National Oceanic and Atmospheric Administration's VDatum (NOAA, 2019b); SA, spatial autocorrelation.

2.3.1. Flooding level

An important first step for this effort was to determine what flooding level should be used for irregularly flooded wetlands. Cowardin et al. (1979) broadly defines irregularly flooded wetlands as those where the land surface is flooded by tidal inundation less than daily. Irregularly flooded wetlands along the northern

Gulf of Mexico are often found above MHW (i.e., the average of all the high water heights observed over the current National Tidal Datum Epoch; 1983–2001) and below the extreme high water spring tide (i.e., increased tide as the result of the Moon being new or full; Cowardin et al., 1979). In addition to regular tides, perigean spring tides, wind-induced water fluctuations, and storms can all play a major role in regulating the salinity and zonation of coastal wetlands, especially in microtidal areas with frequent extreme storms, such as the northern Gulf of Mexico (Stout, 1984). Examples of irregularly flooded wetlands along the Gulf of Mexico are shown in Figure 3.

Fig. 3 Examples of irregularly flooded wetlands along the northern Gulf of Mexico coast, USA. **a** *Spartina patens* (saltmeadow cordgrass) marsh. **b** marsh with *Juncus roemerianus* (black needlerush), and *Distichlis spicata* (saltgrass) with a salt panne in the background. Both photos were taken by Heather Levy in the Florida Big Bend region and used with permission. **c** *Avicennia germinans* (black mangrove) and *Spartina patens* marsh in coastal Louisiana. Photographs by Nicholas Enwright.

NOAA has categorized high-tide flooding into three coastal flooding levels, which include minor flooding (also called nuisance flooding), more severe, storm-driven, moderate flooding, and major flooding (Sweet et al., 2018). NOAA's high-tide flooding levels have been calculated for tide gauges. We assigned high-tide flooding levels to each watershed based on proximity to the nearest NOAA gauge with an assigned high-tide flooding level. We used the minor flooding level for most of the study area as the upper

boundary for irregularly flooded wetlands. The rationale for using NOAA's minor high-tide flooding level is that it captures the extreme spring tide along with perigean spring tides, wind-induced water level fluctuations, and minor storm tides that are often associated with irregularly flooded wetlands, such as high marsh and salt pannes/flats (USNVC, 2022a, b). In addition to high marsh and salt pannes/flats, our definition may include areas that fall within the wetland-upland transition zone (e.g., Thorne et al., 2016). In addition to justification from past literature (Stout, 1984), the use of these flooding levels is in line with recent coastal vegetation elevation analyses in Mississippi (Anderson et al, 2022). This study found the ecotone zone (i.e., wetland to upland transition) in Grand Bay, Mississippi had a maximum elevation of 0.69 m NAVD88. In comparison, the NOAA minor high-tide flooding level for Grand Bay is 0.81 m NAVD88 (using tidal datum transformation for NOAA station ID: 8740166; note, this does not account for any uncertainty from the tidal datum transformation or the NOAA high-tide flooding level). With communication from local experts (Jennifer Wilson and Jena Moon, U.S. Fish and Wildlife Service, oral communication, [September 13, 2021)]), we used the moderate high-tide flooding level for the Laguna Madre and Texas Mid-Coast regions. A higher flooding level was used due to the presence of high marsh and salt pannes/flats at higher elevations, specifically salty prairie in the Texas' upper and middle coast and hypersaline salt flats in South Texas.

2.3.2 Monte Carlo simulations

Using an approach similar to one used by Enwright et al. (2018), we used Monte Carlo simulations run with lidar-derived, hydroflattened DEMs, existing coastal wetland land cover data, tide information, flooding levels, and elevation uncertainty estimates to calculate the probability of an area being irregularly flooded. We used the best available DEMs, which mostly included 1-m DEMs from the USGS 3DEP. Figure 4 shows the acquisition year of lidar used to create DEMs, if known. The point spacing and expected accuracy of lidar data can be characterized using USGS lidar quality levels (USGS, 2022). Of the lidar data used, around 11% of the data had a quality level 1 ($\geq$ 8 points per m^2; 10 cm root mean square error [RMSE] for vertical accuracy; DEM spatial resolution was 1 m or better), 55% was quality

level 2 (≥ 2 points per m^2; 10 cm RMSE for vertical accuracy; DEM spatial resolution was 1 m), 20% was quality level 3 (≥ 0.5 points per m^2; 20 cm RMSE for vertical accuracy; DEM spatial resolution was 3 m), 7% was quality level 4 (139 cm RMSE for vertical accuracy; DEM spatial resolution was ≥ 3 m). Generally, the quality level is linked to year of collection with newer data often having a quality level of 2 or better. Additional details on the DEM source metadata are included in Enwright et al. (2022). We used NOAA's VDatum v4.0 (NOAA, 2019b) to transform the vertical datum of the DEMs at a spatial resolution of 10 m from the NAVD88. Specifically, VDatum was used to create DEMs that were referenced to two locally relevant tidal datums — the mean higher high water and MHW tidal datums.

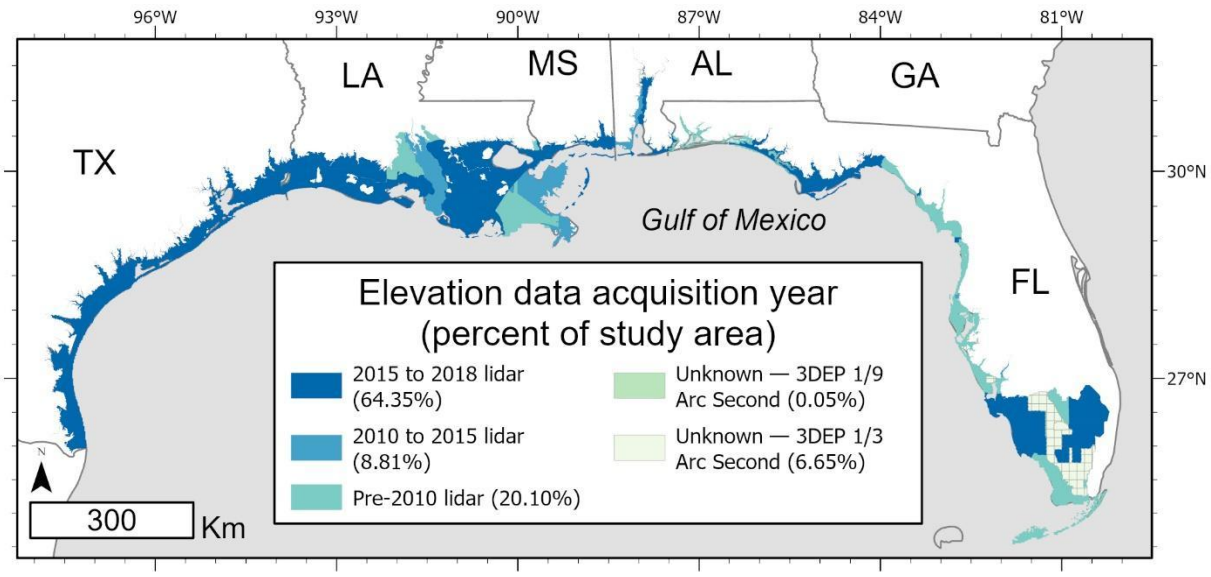

Fig. 4. Acquisition year for elevation data used to estimate the irregularly flooded wetland probability along the northern Gulf of Mexico coast, USA. 3DEP, U.S. Geological Survey's 3D Elevation Program (USGS, 2020).

Monte Carlo simulations included 1,000 iterations and were used to determine if pixel elevation was above MHW and below high-tide flooding levels (Sweet et al., 2018) while propagating various sources of elevation uncertainty. Elevation uncertainty included literature-derived estimates of coastal wetland

elevation error in lidar data, regionally variable tidal datum uncertainty from VDatum, and the high-tide flooding level uncertainty. Regional VDatum uncertainty estimates were assigned to watersheds via the VDatum region that covered the majority of the watershed. The NOAA high-tide flooding level uncertainty had a RMSE of 0.19 m and 0.25 m for minor and moderate high-tide flooding levels, respectively (Sweet et al., 2018). To increase computational efficiency, all elevation values and elevation uncertainty estimates used in this study were multiplied by 1,000 and converted to integer (Appendix A).

As previously mentioned, we conducted a literature review to derive estimates of coastal wetland elevation error in lidar data. For this review, we documented the pulse spacing, elevation error, ground truth source, and study location (Appendix A). To be conservative, we truncated the literature-derived coastal wetland elevation error estimate to cm precision (i.e., 0.23 m) and multiplied by 1,000 (i.e., 230).

For each region, we estimated the Euclidean distance where there was no spatial autocorrelation in coastal wetland elevation. We used GeoDa v. 1.20 (Anselin et al., 2006) to develop spatial correlograms for each watershed with 40 distance bins for elevation data resampled to 100 m. We determined the distance bins where the spatial autocorrelation intersected the zero intercept and determined the average of the two distance bins (e.g., Figure S1). We calculated the median distance for where no spatial autocorrelation existed per region.

For each iteration in the Monte Carlo simulation, a random field was created by developing a random raster with a normal distribution that had mean set to 0 and the SD set to the coastal wetland elevation error estimate (i.e., 230 [0.23 m]). Because elevation error in DEMs for coastal wetlands is mostly positive (Buffington et al., 2016; Kidwell et al., 2017; Enwright et al., 2018; Alizad et al., 2020), we forced the error to be positive for 95% of the iterations by taking the absolute value of the random field. We left the bias of the error unconstrained for remaining 5% of the iterations. The spatial resolution of this raster was set to the zero spatial autocorrelation distance for the respective region for the watershed.

Next, the random field was converted to a point shapefile. We used inverse distance weighted interpolation to develop a 10-m rasterized random field from the point shapefile. In addition to uncertainty related to coastal wetland elevation, the Monte Carlo simulations also integrated uncertainty for the upper and lower bounds of the irregularly flooded wetland zone (Table S1). For each iteration, the upper and lower bounds were permuted using a random number from a normal distribution with a mean of zero and a standard deviation set to the uncertainty values (Table S2).

2.3.3 Binning probabilistic outputs

The watershed-based probability layers were mosaicked into a single raster file for the northern Gulf of Mexico. To summarize areal coverage of probability ranges, we reclassified the continuous probability layer that ranged from 0–1 into three classes that are used by the Intergovernmental Panel on Climate Change for communicating probabilities (IPCC, 2022). The first class includes areas that are unlikely to be irregularly flooded wetlands (probability ≤ 0.33). The second class includes areas that are as likely as not to be irregularly flooded wetlands (probability > 0.33 and ≤ 0.66). The final class includes areas that are likely to be irregularly flooded wetlands (probability > 0.66). We used the midpoint of the NOAA high-tide flooding level and the MHW tidal datum to estimate whether areas that were unlikely to be irregularly flooded wetlands (i.e., probability ≤ 0.33) were in the upper (higher) or lower portion of the irregularly flooded wetland zone. We summarized the absolute and relative coverage of irregularly flooded wetlands by class by region and watershed (Fig. 1).

2.4. Probabilistic output validation

We used in situ elevation observations collected between 2012 and 2021 within coastal wetlands (n = 3,027) referenced to NAVD88 from a variety of sources across the northern Gulf of Mexico coast to validate the irregularly flooded wetland probability layer (Table 1). Points were located in every region except the Florida Panhandle. Some data came from Online Positioning User Service (OPUS) survey points and National Geodetic Survey benchmarks (Table 1; Stoker and Miller, 2022). For benchmark data,

we restricted the points to those with an elevation source labelled as either "leveling" and "GPS observation." These data have been used for other landscape-scale lidar DEM accuracy assessments (Gesch et al., 2014; Stoker and Miller, 2022).

While these in situ data may not have been collected at the same time as the lidar elevation data, these data provide a reasonable approach to validating the probabilistic outputs and are in line with the general approach of using the best available data, especially given the spatially extensive nature of the study area. While studies often compare a DEM to in situ elevation data using linear regression (Stoker and Miller, 2022; Medeiros et al., 2022), we opted to use a Spearman's rank correlation to show the relationship between the probability of an area being irregularly flooded estimated using the DEMs and the in situ observations due to the constraint for linear regression having no spatial autocorrelation of the residuals, which is often violated in spatial environmental datasets. We conducted correlation analyses for the entire Gulf of Mexico coast and by region for regions with over 30 data points (Table 1). We developed box plots for the difference and absolute difference between the probability values from the DEMs and the in situ points and calculated the mean bias error (MBE), mean absolute error (MAE), and the root mean square error (RMSE). All plots were created in SigmaPlot 12.5 (SyStat Software Inc.; San Jose, California, USA).

$$MBE = \frac{\sum_{i=1}^{n} (P_i - O_i)}{n} \quad (2)$$

$$MAE = \frac{\sum_{i=1}^{n} |P_i - O_i|}{n} \quad (3)$$

$$RMSE = \sqrt{\frac{\sum_{i=1}^{n} (P_i - O_i)^2}{n}} \quad (4)$$

where P_i is the irregularly flooded wetland probability value from the DEMs, O_i is the irregularly flooded wetland probability value from in situ observations, n is the number of validation points, and *i* is an

integer from 1 to n. These statistics have been used by other studies for comparing elevation data and in situ observations (e.g., ASPRS, 2015; Cooper et al., 2019; Stoker and Miller, 2022; Medeiros et al., 2022). All validation results were rounded to the nearest cm.

Table 1. In situ elevation sources, number of points per source, and total points by region for comparison with the irregularly flooded wetland probability along the northern Gulf of Mexico coast, USA. See Figure 1 for regional boundaries**.**

Region	Source(s)	Points per source	Region total
Laguna Madre	Stoker and Miller (2022)	12	12
Texas Mid-Coast	Moon et al. (2022)	9	180
	Stagg et al. (2021)	161	
	Stoker and Miller (2022)	10	
Chenier Plain	Moon et al. (2022)	5	706
	Sharp et al. (2021)	669	
	Stagg et al. (2020)	29	
	Stoker and Miller (2022)	3	
Mid-Deltaic Plain	Sharp et al. (2021)	347	349
	Stoker and Miller (2022)	2	
Deltaic Plain	Sharp et al. (2021)	609	612
	Stoker and Miller (2022)	3	
Mississippi Sound	Andrews (2022)	124	915
	Brunden et al. (in review)	532	
	Medeiros et al. (2022)	95	
	Sharp et al. (2021)	161	
	Stoker and Miller (2022)	3	
Florida Big Bend	Medeiros et al. (2022)	85	93
	Stoker and Miller (2022)	8	
West Peninsula Florida	Buffington and Thorne (2022)	88	101
	Stoker and Miller (2022)	13	
Everglades	Buffington and Thorne (2022)	53	53
Florida Keys	Stoker and Miller (2022)	6	6

In addition to an overall assessment, validation was conducted for several categories including by lidar acquisition year bins, lidar quality levels, and land cover classes. Lidar acquisition year bins included: (1) pre-2005; (2) 2005–10; (3) 2010–15; and (4) 2015–18. The validation was assessed for individual lidar quality levels, except for levels 3 and 4, which were combined. Finally, we assessed the validation for the following land cover classes from 2016 30-m C-CAP land cover data: (1) estuarine emergent marsh; (2)

estuarine woody wetland, with included both forested and scrub-shrub wetlands; (3) palustrine emergent marsh; (4) palustrine woody wetland, with included both forested and scrub-shrub wetlands; and (5) nonvegetated, which included unconsolidated shore, water, and palustrine and estuarine aquatic bed wetlands. For the landcover analysis, we omitted 10 points that were not mapped as one of the previously mentioned classes in the 2016 30-m C-CAP land cover map. Note, this rare event was caused by the coastal wetland mask being developed from both the 30-m C-CAP land cover product and the 2016 10-m C-CAP BETA land cover product.

3. Results

3.1. Irregularly flooded wetland probability and validation

The output of the irregularly flooded wetland probability analysis was a spatially explicit probabilistic raster that was published as a USGS data release (Enwright et al., 2022). For this product, we utilized lidar error from literature for coastal wetland DEMs from 23 different studies, which had a mean value of 0.46 m with an outlier (1.27 m linear error at 95% confidence) removed (Appendix A; Table S3). An example of the data around Grand Bay, Mississippi is shown in Figure 5.

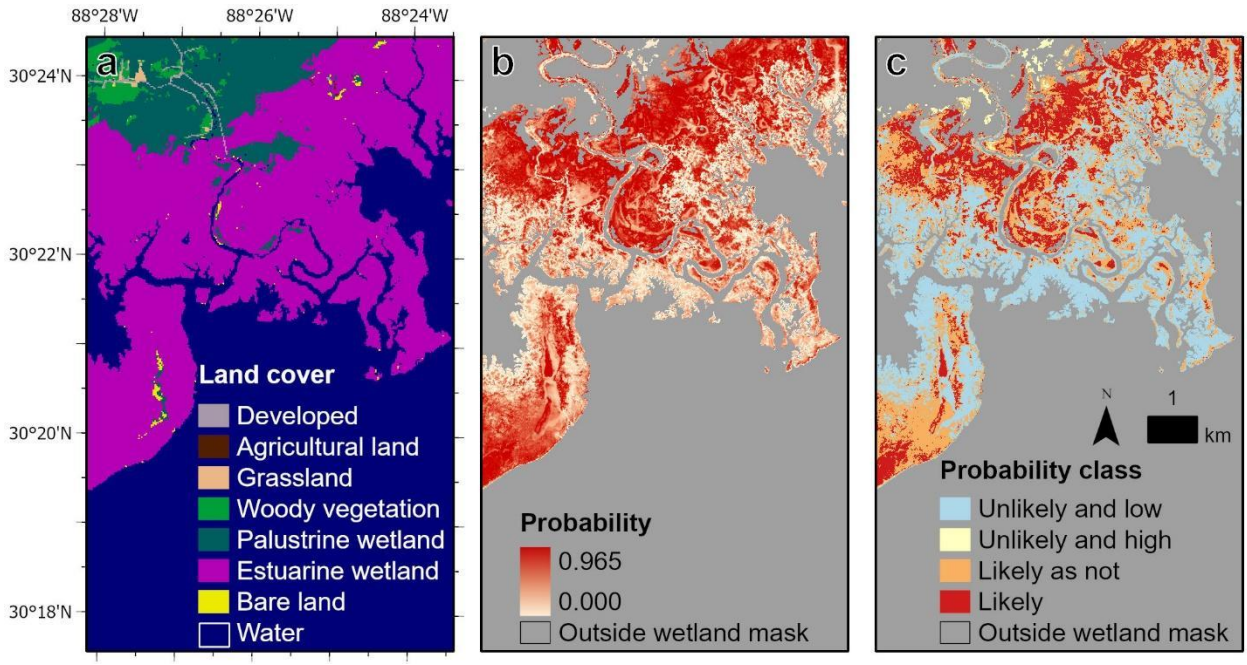

Fig. 5. Example of the irregularly flooded wetland probability output near Grand Bay, Mississippi, USA. **a** land cover map modified from the National Oceanic and Atmospheric Administration's Coastal Change Analysis Program 30-m layer (NOAA, 2016). **b** irregularly flooded wetland probability on a continuous scale for areas within the coastal wetland mask. **c** irregularly flooded wetland probability by percent bin for areas within the coastal wetland mask. Unlikely and low, probability ≤ 0.33 and below mid-point between mean high water and the NOAA high-tide flooding level (Sweet et al., 2018); Unlikely and high, probability ≤ 0.33 and above mid-point between mean high water and the NOAA high-tide flooding level; Likely as not, probability > 0.33 and ≤ 0.66; Likely, probability > 0.66.

In situ elevation data were used to validate the irregularly flooded wetland product. The results of the Spearman's correlation analysis found that there was a moderate positive correlation ($r = 0.563$, $p < 0.0001$) between the probability estimated from the in situ elevation data and probability estimated from the DEMs. When exploring the probability differences, the MBE was around -0.04 (i.e., in situ-based probability was slightly higher than DEM-based probability), the MAE was 0.20, and the RMSE was 0.26 (Fig. 6).

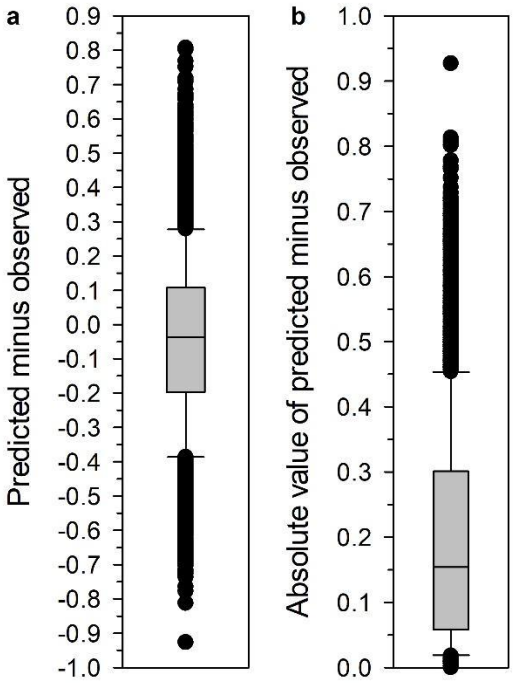

Fig. 6. Box plots for the difference in probability for being an irregularly flooded wetland (digital elevation model-based probability minus in situ observation-based probability) along the northern Gulf of Mexico, USA (n = 3,027). **a** raw difference, **b** absolute value of the difference.

The relationship between the DEM-based probability and in situ-based probability varied by region (Fig. 7). The relationship between probability estimates for the Texas Mid-Coast region was not significant (n = 180; r = 0.057; p > 0.05). Due the lack of a relationship, the MBE, MAE, and RMSE were calculated for this region, which were -0.17, 0.26, 0.34, respectively. There was a positive relationship between DEM-based probability and in situ-based probability for all other regions. The Spearman's correlation coefficients ranged from 0.399 (Deltaic Plain) to 0.702 (Florida Big Bend) with a $p < 0.0001$. The points for some regions in Florida (i.e., Florida Big Bend, West Peninsula Florida, and Everglades) did not cover the full range of probabilities (Fig. 7).

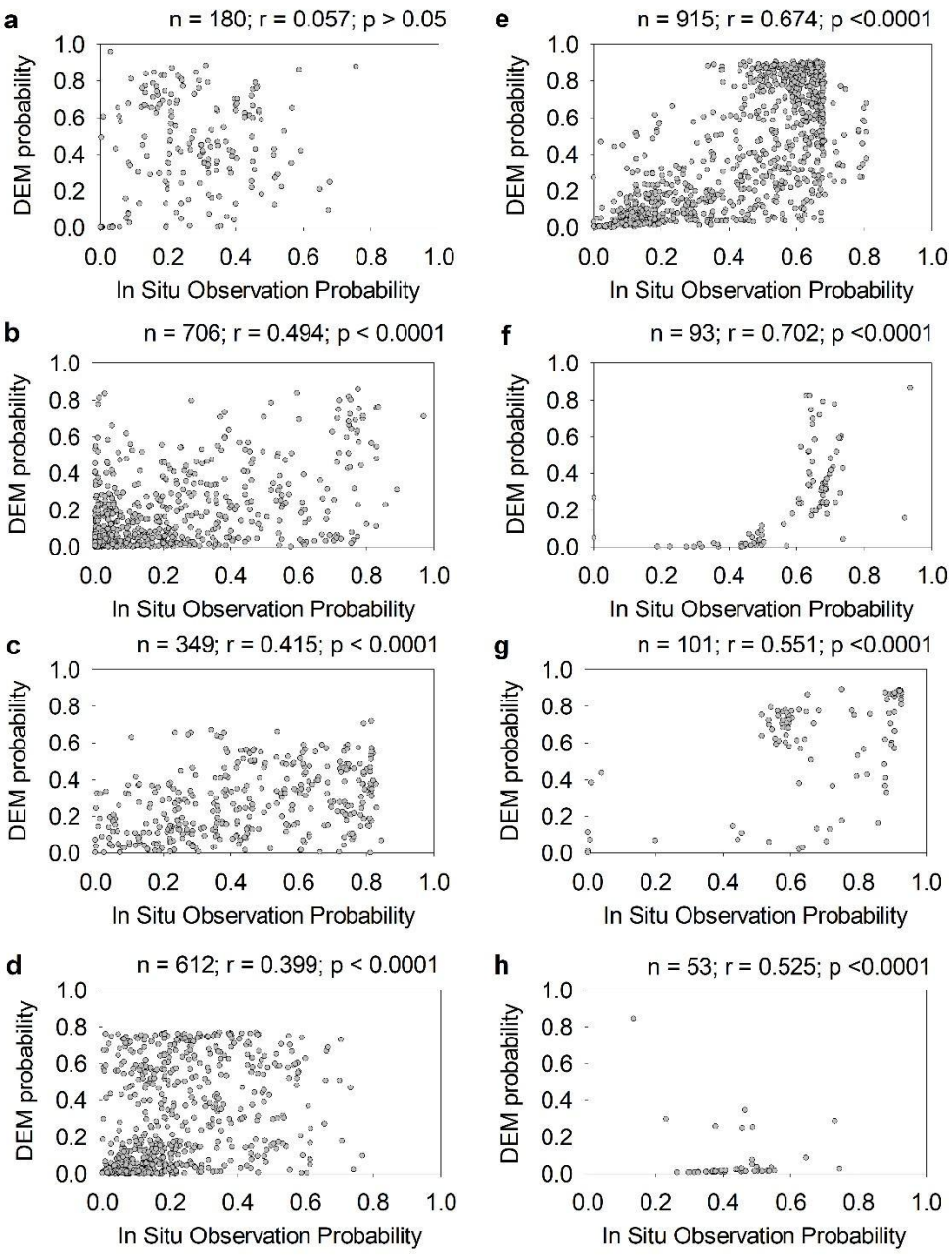

Fig. 7. Scatter plots and Spearman's correlation coefficients between the irregularly flooded wetland probability estimated from the in situ elevation observations and from the DEMs by region along the northern Gulf of Mexico coast, USA. **a** Texas Mid-Coast, **b** Chenier Plain, **c** Mid-Deltaic Plain, **d** Deltaic Plain, **e** Mississippi Sound, **f** Florida Big Bend, **g** West Peninsula Florida, **h** Everglades. Region-specific analysis was not conducted for regions with less than 30 points. See Figure 1 for regional boundaries.

In general, older lidar data and lidar with a lower quality level seemed to have less agreement between the probabilistic estimates from the DEMs and in situ observations (Table 2). Compared to newer lidar acquisitions, validation from lidar acquired prior to 2010 had a greater magnitude for all error metrics. The validation results for lidar quality levels generally tracked the lidar acquisition year results. Most of the validation data fell within the estuarine emergent wetland class (about 78% of the points). Validation for the estuarine emergent wetland and palustrine emergent wetland had similar results for all metrics. Estuarine and palustrine woody had the highest correlation coefficients. In general, the error metrics for woody and nonvegetated had the highest magnitude error, whereas error metrics for palustrine woody were similar to emergent marsh. Nonvegetated had the lowest correlation coefficient of all land cover types.

Table 2. Validation of irregularly flooded wetland probability estimates from digital elevation models along the northern Gulf of Mexico coast, USA using in situ elevation observations. The Spearman's coefficient was only calculated for categories with more than 30 points. *, $p < 0.001$; MBE, mean bias error; MAE, mean absolute error; RMSE, root mean square error, NA; not applicable.

Validation	Category	n	Spearman's coefficient	MBE	MAE	RMSE
All points	NA	3,027	0.563*	-0.04	0.20	0.26
Acquisition years	pre-2005	232	0.036	0.25	0.31	0.37
	2005–10	13	NA	-0.24	0.30	0.39
	2010–15	261	0.469*	-0.01	0.15	0.21
	2015–18	2,521	0.615*	-0.07	0.19	0.25
Lidar quality levels	1 (≥ 8 points per m^2)	160	0.805*	-0.17	0.24	0.31
	2 (≥ 2 points per m^2)	2,361	0.613*	-0.07	0.19	0.25
	3–4 (≥ 0.5 points per m^2)	506	0.388*	0.11	0.23	0.30
Land cover classes (omitting five non-wetland classes)	Estuarine emergent marsh	2,350	0.570*	-0.03	0.19	0.25
	Estuarine woody	84	0.719*	-0.18	0.25	0.32
	Palustrine emergent marsh	380	0.545*	-0.09	0.20	0.28
	Palustrine woody	68	0.740*	-0.08	0.15	0.20
	Nonvegetated	135	0.424*	-0.14	0.26	0.33

3.3. Irregularly flooded wetland probability areal coverage

To quantify and explore differences in areal coverage along the northern Gulf of Mexico, we classified the probability values into three equal bins and evaluated whether wetlands in the lowest bin (probability ≤ 0.33) were in the lower or upper (higher) portion of the irregularly flooded zone (Table 3). Most of the area under the coastal wetland mask was included in either one of the unlikely classes (i.e., unlikely and low and unlikely and high). This area was closely divided between the two classes with around 10,355.86 km^2 (~38%) of the coastal wetland mask classified as unlikely and low and 9,024.94 km^2 (~33%) of the coastal wetland mask classified as unlikely and high. The majority of the area classified as unlikely and low was located in Louisiana (Table S4). For this class, the top-five regions based on areal coverage were: (1) Chenier Plain, 3,124.05 km^2 (~30% of the Gulf total); (2) Deltaic Plain, 2,179.66 km^2 (~21% of the Gulf total); (3) Mid-Deltaic Plain, 1,744.01 km^2 (~17% of the Gulf total); (4) Everglades, 1,058.12 km^2 (~10% of the Gulf total); and (5) Mississippi Sound, 815.47 km^2 (~8% of the Gulf total). Most of the area classified as unlikely and high was in the Everglades region (Table 3). For this class, the top-five regions based on areal coverage were: (1) Everglades, 6,420.03 km^2 (~71% of the Gulf total); (2) Texas Mid-Coast, 1,153.16 km^2 (~13% of the Gulf total); (3) Laguna Madre, 726.63 km^2 (~8% of the Gulf total); (4) Deltaic Plain, 251.05 km^2 (~3% of the Gulf total); and (5) Chenier Plain, 187.49 km^2 (~2% of the Gulf total).

About 3,411 km^2 (~13% of the area under the coastal wetland mask) was classified as likely to be an irregularly flooded wetland. Most of this area was in Florida, Texas, and Louisiana (Tables 3). For this class, the top-five regions based on areal coverage were: (1) Everglades, 1,104.46 km^2 (~32% of the Gulf total); (2) Chenier Plain, 520.96 km^2 (~15% of the Gulf total); (3) Texas Mid-Coast, 385.15 km^2 (~11% of the Gulf total); (4) Laguna Madre, 369.41 km^2 (~11% of the Gulf total); and (5) Deltaic Plain, 354.97 km^2 (~10% of the Gulf total). A breakdown of the areal coverage of irregularly flooded wetland probability by watershed is found in Table S4.

Table 3. Areal coverage irregularly flooded wetland probability by bin by region along the northern Gulf of Mexico, USA. Unlikely and low, probability ≤ 0.33 and below mid-point between mean high water and the NOAA high-tide flooding level (Sweet et al., 2018); Unlikely and high, probability ≤ 0.33 and above mid-point between mean high water and the NOAA high-tide flooding level; Likely as not, probability > 0.33 and ≤ 0.66; Likely, probability > 0.66. See Figure 1 for regional boundaries.

	Coverage irregularly flooded wetland probability (km^2)				
Region	**Unlikely and low**	**Unlikely and high**	**Likely as not**	**Likely**	**Total**
Laguna Madre	165.31	726.63	425.16	369.41	1,686.51
Texas Mid-Coast	436.12	1,153.16	484.20	385.15	2,458.63
Chenier Plain	3,124.05	187.49	758.88	520.96	4,591.38
Mid-Deltaic Plain	1,744.01	10.74	494.49	105.73	2,354.98
Deltaic Plain	2,179.66	251.05	760.01	354.97	3,545.69
Mississippi Sound	815.47	74.29	181.70	98.19	1,169.65
Florida Panhandle	72.25	75.27	46.58	72.78	266.88
Florida Big Bend	515.58	49.62	156.20	195.16	916.56
West Peninsula Florida	190.07	69.49	166.51	161.44	587.51
Everglades	1,058.12	6,420.03	594.46	1,104.46	9,177.06
Florida Keys	55.22	7.17	48.20	42.78	153.37
Gulf-wide	10,355.86	9,024.94	4,116.39	3,411.03	26,908.22

Beyond overall coverage, regional comparisons using relative coverage differences for each bin by region can provide additional insight in the general distribution and coverage of irregularly flooded wetlands (Fig. 8). For the unlikely and low bin, the top-five regions based on relative areal coverage (rounded to nearest percentage) were: (1) Mid-Deltaic Plain, 74%; (2) Mississippi Sound, 70%; (3) Chenier Plain, 68%; (4) Deltaic Plain, 61%; and (5) Florida Big Bend, 56%. For the unlikely and high bin, the top-five regions based on relative areal coverage (rounded to the nearest percentage) were: (1) Everglades, 70%; (2) Texas Mid-Coast, 47%; (3) Laguna Madre, 43%; (4) Florida Panhandle, 28%; and (5) West Peninsula Florida, 12%. For the remaining area under the coastal wetland mask, there was about 15% in the likely as not class and 13% in the likely class. For likely class, the top-five regions based on relative areal coverage (rounded to the nearest percentage) were: (1) Florida Keys, 28%; (2) Florida Panhandle, 27%; (3) West Peninsular Florida, 27%; (4) Laguna Madre, 22%; and (5) Florida Big Bend, 21%.

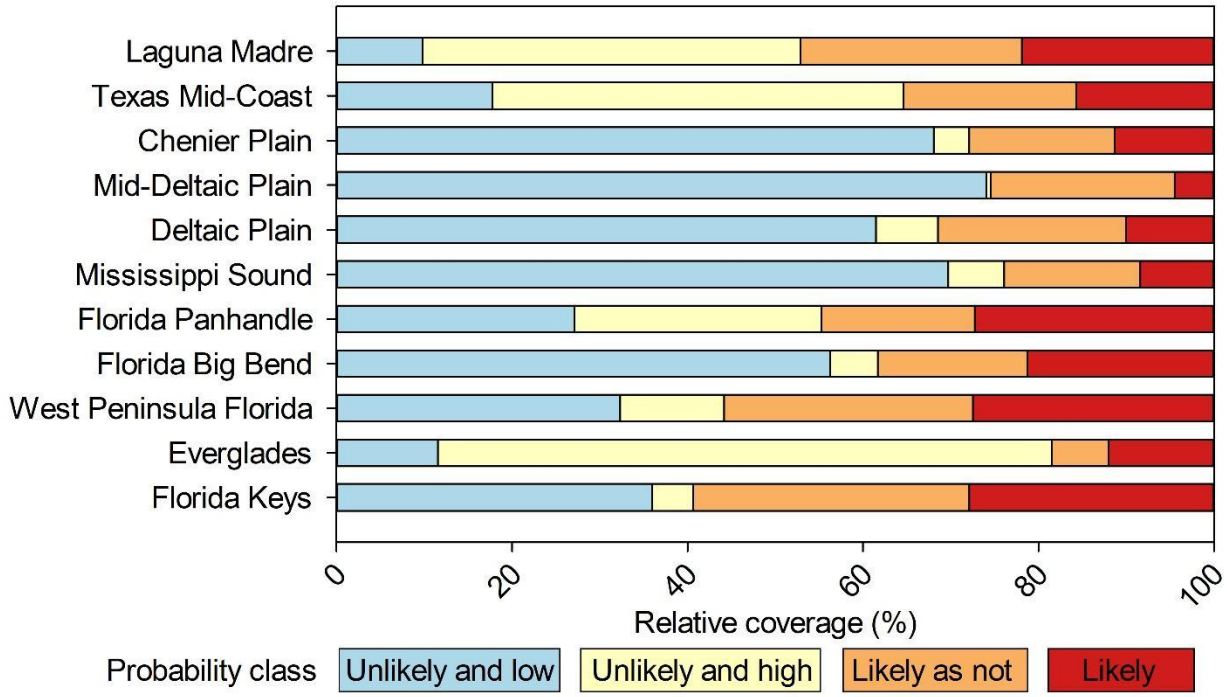

Fig. 8. Relative coverage of irregularly flooded wetland probability by percent bin for regions along the northern Gulf of Mexico, USA. Unlikely and low, probability ≤ 0.33 and below mid-point between mean high water and the NOAA high-tide flooding level (Sweet et al., 2018); Unlikely and high, probability ≤ 0.33 and above mid-point between mean high water and the NOAA high-tide flooding level; Likely as not, probability > 0.33 and ≤ 0.66; Likely, probability > 0.66. See Figure 1 for regional boundaries.

4. Discussion

The primary objective of this study was to develop a framework for estimating irregularly flooded wetland probability using NOAA's high-tide flooding levels. While the outputs of this study are similar to the work by Holmquist and Windham-Myers (2022) regarding the use of uncertainty to produce regional maps related to wetland inundation zonation, our product is the first regional map of elevation-based irregularly flooded wetland probability across the northern Gulf of Mexico coast. This product can serve many important applications including providing a baseline for gauging future coastal wetland change

with climate change and designing wetland vegetation and faunal monitoring programs (e.g., above-ground biomass transects and developing marsh bird surveys).

4.1. Interpretations and applications

The results from the analysis provide a snapshot of irregularly flooded wetland probability distribution across the region. Overall, these results are aligned with past efforts to quantify wetland coverage in the Gulf of Mexico and highlight abundant wetland coverage in low-lying areas in south Louisiana and south Florida (Reyer et al., 1988; Table 3). By using various sources of uncertainty, the probabilistic outputs add helpful nuance to simply quantifying the areal coverage of coastal wetlands by region or watershed. These results can be used to address questions such as what watersheds or regions have a high abundance of areas that are: (1) likely to be irregularly flooded wetland; (2) unlikely to be irregularly flooded wetland and low elevation; and (3) unlikely to be irregularly flooded wetland and high elevation.

Based on our results, we found that the Everglades and coastal watersheds from south Texas to southwestern Louisiana have abundant areas that are likely irregularly flooded wetland. We found south Louisiana and the Everglades have a high amount of area classified as unlikely to be irregularly flooded wetland and low. Finally, we found that the Everglades, Texas Mid-Coast, and Laguna Madre were regions have a high abundance of areas classified as unlikely to be an irregularly flooded wetland and high. Collectively, these results can provide information on the regional variability of coastal wetlands and provide general insights into how the wetlands in a region may be able to adapt to or withstand sea-level rise. For example, depending upon localized sediment accretion and subsidence rates, a watershed with an abundance of area mapped as likely to be irregularly flooded wetland or unlikely to be irregularly flooded wetland and high may have an increased capacity to adapt to future sea-level rise compared to regions that have a large amount of area that is unlikely to be irregularly flooded wetland and low (Saintilan et al., 2022). Areas that are mapped as unlikely to be irregularly flooded wetland and low may be candidates for placement of beneficial use materials to increase wetland elevation or, if

impounded, tidal restoration to increase the frequency of sedimentation via tidal influence (Zhao et al., 2016). Likewise, regions that have abundant area classified as unlikely to be irregularly flooded wetland and high include areas that are currently mapped as coastal wetland but are located further upslope in freshwater wetlands. These areas include wetlands that may be irregularly flooded in the future with sea-level rise (Osland et al., 2022). Our understanding of the ability for coastal wetland adaptation or transformation may be expanded by combining the probabilistic layers developed in this study with coastal wetland condition metrics such as the unvegetated-vegetated ratio, which are correlated with wetland sediment budgets and wetland sea-level rise response (Ganju et al., 2022). Additionally, irregularly flooded marsh provides important habitat for many coastal fauna, such as the Eastern Black Rail (*Laterallus jamaicensis jamaicensis*; Tolliver et al., 2018), which was listed as threatened by the U.S. Fish and Wildlife Service in 2020. Maps of irregularly flooded wetland coverage can help assist land managers with habitat mapping for wetland-reliant fauna and develop current and future species-focused conservation plans (Moon et al., 2021).

With accelerated sea-level rise, the frequency of the occurrence of the NOAA high-tide flooding levels used in this study is expected to increase over the next several decades, with an especially high magnitude increase in frequency along the northern Gulf of Mexico occurring in the 2030s (Sweet et al. 2018; Thompson et al., 2021). As previously mentioned, this map can provide insights into potential adaptive capacity of current wetlands for sea-level rise. Rising sea level associated with climate change is expected to lead to wetland loss and transformation (Osland et al., 2022). Therefore, there is a need for repeatable methods, such as the approach used in this study, to observe changes in irregularly flooded wetland probability over time. Change assessments between maps of irregularly flooded wetland probability could incorporate algorithms that are robust to noise, such as those that commonly used for detecting meaningful coastal geomorphic change by using mean and standard deviation of values (e.g., probabilities) between time periods (e.g., Liu et al., 2010). In addition to mapping contemporary irregularly flooded wetlands, the approach used in this study could be expanded to map potential future

irregularly flooded wetlands using NOAA high-tide flooding levels and sea-level rise scenarios. Observations over time and projections can provide researchers with the ability to validate and refine wetland transformation models.

Finally, while our approach and product are helpful for identifying coarse wetland zonation based on inundation, the probabilistic outputs from this project could be used for more detailed vegetation-specific analyses. For example, vegetation data could be paired with these probabilistic maps and other remotely sensed data for a variety of analyses including species-level mapping, vegetation community-level mapping, and condition analyses. As an example, these data could be helpful for more detailed vegetation community delineation, such as determining high marsh, which is a subclass of irregularly flooded wetlands that is often dominated by vegetation species such as *Spartina patens* and includes other characteristic species, such as *Distichlis spicata*, *Iva frutescens*, and *Salicornia* spp. (USNVC, 2022a).

4.2. Elevation uncertainty and validation

Due to the well-documented elevation error in lidar data for coastal wetlands (Su and Bork, 2006; Schmid et al. 2011; Medeiros et al., 2015; Buffington et al., 2016), researchers have used a literature review to estimate possible lidar elevation error in coastal wetlands. This can be challenging because the level of detail of the in situ elevation data collection and error reporting may vary by study. Holmquist et al. (2018) published the first such literature review, which included four studies across many sites. The review led to the development of a site-weighted error and other error estimates, which included a mean offset of 0.173 m, a standard error of 0.110 m, and an assumed random error of 0.205 m (Holmquist and Windham-Meyers, 2022). These uncertainties were combined using the sum of squares for an average total uncertainty of 0.233 m. Building on this effort, for 12 studies, Alizad et al. (2020) found a pooled mean lidar error of 0.18 m and a standard deviation of 0.14 m. Our effort added to the literature review for a total of 23 studies. Because vegetation elevation error is often not normally distributed (ASPRS, 2015), we attempted to standardize the error estimates to either the 95th percentile or the linear error at 95%

confidence. We calculated the mean value of the 95th percentile and the linear error at 95% confidence error estimates, which was 0.230 m.

The validation results point to a slight underestimate in probability when estimated from DEMs (MBE = -0.04), which is likely due to overestimating of wetland elevation error for the areas tested. As previously mentioned, older lidar data and data with a lower quality level seemed to have less agreement for the probabilistic estimates from lidar data and in situ observations (Table 2). While this drop in agreement could be due to the lidar spacing, it could also be due to a large temporal gap between in situ elevation observations and lidar acquisition. While quality level 1 data had the highest correlation coefficient, the magnitude of the MBE and MAE was greater compared to quality level 2 data. To add context to these results, around 5% of the validation points were assessed with quality level 1 lidar, whereas about 78% of the points were from quality level 2 lidar. Due to the limited number of points linked to quality level 1 lidar data, additional data analysis for both quality levels could help better elucidate the differences in results between these two quality levels. Likewise, although woody wetland classes appeared to have a stronger correlation, additional data analysis for non-marsh wetlands could help reveal the validation differences by wetland types and provide more targeted information for elevation error in non-marsh wetlands. While this study estimated correlation by region, future efforts could expand on how regional differences in geomorphology, climate, and management of coastal lands impact irregularly flooded wetland delineation and validation using high-quality vegetation and in situ elevation data that was collected in a similar time period as the lidar acquisition. Despite a moderate correlation result and slight underestimate in probability, the product produced in our study provides the best available dataset for the probabilistic estimate of irregularly flooded wetland coverage at the landscape scale and can be used for the previously mentioned applications.

4.3. Expanding upon past efforts

Holmquist and Windham-Myers (2022) calculated relative tidal elevation for the conterminous United States, which focused on wetlands below the MHHWS tidal datum. Their products include an estimate of the relative position in the tidal range and delineate regularly flooded wetlands (i.e., "low marsh;" areas exposed to tides daily). Our product complements the work done by Holmquist and Windham-Myers (2022) by focusing on the irregularly flooded wetland zone. In our study, we also produced a probabilistic coastal wetland map; however, we bracketed the irregularly flooded wetland zone with MHW as the lower bound and NOAA high-tide flooding levels as the upper bound. As previously mentioned, the NOAA high-tide flooding level includes inundation associated with perigean spring tides, wind-induced water fluctuations, and minor storms and was aligned with the U.S. National Vegetation Classification high marsh and salt panne/flat definitions. As previously mentioned, the use of a higher threshold was aligned with flooding levels used by Brophy et al. (2019), which aimed at delineating estuarine boundaries using lidar data, and field observations by Anderson et al. (2022).

In our study, we used Monte Carlo simulations to address uncertainty and develop probabilistic outputs, whereas Holmquist and Windham-Myers (2022) propagated uncertainty using partial derivatives. A strength of the Monte Carlo approach is that it utilizes spatial random fields for propagating the coastal wetland elevation error. Our effort built on past research that used local spatial autocorrelation via a 3-by-3-pixel filter (Enwright et al., 2018) and a multi-scaled approach using six different box sizes thought to potentially represent possible spatial autocorrelation of elevation error in coastal areas (Kulp and Strauss, 2019). In this study, we used the distance that spatial autocorrelation of coastal wetland elevation was zero. We also added interpolation to develop smooth random fields between the coarser spatial autocorrelation-based box sizes as suggested by Wechsler and Kroll (2006). The use of spatial autocorrelation of coastal wetland elevation was informed by findings by Alizad et al. (2020), which found that wetland elevation error in lidar datasets in some areas, such as Plum Island, Massachusetts, generally tracks with wetland elevation. While the use of coastal wetland elevation spatial autocorrelation

was a helpful starting point, wetland elevation error in lidar can be spatially variable and depend on species and vegetation height (Buffington et al., 2016; Alizad et al., 2020).

For sea-level rise studies, a general rule of thumb is that confidence in accurately mapping inundation increases with higher thresholds due to less overlap with the target inundation level and elevation uncertainty in source data (Gesch, 2018). This can introduce challenges with contemporary tidal wetland mapping as tidal datums, such as MHW or MHHWS, which may not be outside the uncertainty of the lidar, especially for microtidal areas like the northern Gulf of Mexico (Alizad et al., 2020; Holmquist and Windham-Myers, 2022). Likewise, it could be difficult to find the probability of wetlands falling between narrow tidal datums (e.g., wetlands between MHW and MHHWS). The use of a wider inundation zone in our study (i.e., MHW as lower bound and around 0.5 m to 0.8 m above MHHW as the upper bound) may have helped alleviate some of these issues. While the lidar vertical error may impact the probability results for the lower end of the zone (i.e., wetlands that are at or near the MHW datum), the width of this zone can help increase the confidence in the probabilistic results in the rest of the zone. Holmquist and Windham-Myers (2022) did not set an upper bound for the high class or the Z*MHW, but instead used wetland data to limit the area to estuarine wetlands, palustrine wetlands that were thought to be below MHHWS, and tidal wetlands. Differences in approach, data availability at the time of analysis, and research questions between Holmquist and Windham-Myers (2022) and our study prevent a meaningful direct comparison of products produced; however, the differences between the approaches and research questions make the products from both studies complementary.

4.4. Limitations and additional next steps

As previously mentioned, older lidar data and lidar data with a lower quality level seemed to have reduced the agreement between the probabilistic estimates from lidar data and in situ elevation observations. While most of the study area included recent data collections with a quality level 2, there were two locations were older lidar data were used. The best available elevation data at the time this study

was conducted was 3DEP 1/3 arc second data (parts of the Everglades region) and lidar data with questionable quality in coastal wetlands (parts of the Deltaic Plain region). The impact of the disparate data sources created anomalous results (i.e., unlikely straight lines/breaks in probability). New lidar data from 2018 are now available for most of Florida and there is a recent acquisition for the Deltaic Plain of Louisiana that has not yet been published.

While this effort used C-CAP data to develop a coastal wetland mask, this approach could be modified so that it can be used with any existing land cover product. This could include land cover maps that have reduced thematic detail such as USGS' NLCD, which includes wetlands mapped as either woody wetlands or emergent herbaceous wetlands, or LCMAP, which has a single wetland class. For this study, our coastal wetland mask did not explicitly include palustrine scrub/shrub and palustrine forested wetlands. Future research could explore whether these classes could be added to help identify freshwater forested wetlands that are irregularly exposed to saline water. This may require a more nuanced approach to addressing elevation error in vegetated areas than used in this study. For example, it would be important to ensure that elevation error estimates were developed for specific types of vegetation (e.g., scrub/shrub and forested), which may have a lower elevation error.

In this study, we used available in situ elevation observations, which may have potential for time differences between the lidar acquisition date. The scope of the study area and limited in situ data availability hindered our ability to add constraints for in situ and lidar acquisition related to temporal gaps. For this reason, we also decided to limit our validation efforts to land cover types and not by species or vegetation characteristics (e.g., height and percent cover by species). Future efforts focused on regional analyses could enhance the validation by using stricter constraints on data acquisition timing gaps and factor in vegetation cover and characteristics for probability validation.

Future efforts could include updating this map as new and improved coastal wetland elevation error estimates, new elevation data, and tidal datum transformations (with uncertainty estimates) become available. In this study, we found that lidar data advances, namely increasing points per square meter, have generally led to a reduction in lidar error in coastal wetlands. Future studies could evaluate whether lidar sensor technology advances, such as single photon and Geiger-mode lidar sensors (Stoker et al., 2016), and increased availability in lidar with a quality level 1 or 2 may help reduce lidar error in coastal wetlands. Additionally, the availability of lidar point cloud analysis in cloud-based platforms like Google Earth Engine and Microsoft's Planetary Computer may allow for researchers to efficiently use approaches to extract vegetation height information (Koma et al., 2021), which could enhance our understanding of potential elevation error. Likewise, future efforts could expand on this approach by integrating vegetation biomass or greenness, (Byrd et al., 2018) or vegetation height extraction from lidar point cloud into random fields. For example, salt pannes could have sparse cover and likely have low elevation error, but the approach used in our study did not account for variable vegetation cover. Likewise, areas with tall *Juncus roemerianus* may have higher elevation error than other surrounding vegetation communities like *Spartina patens* or succulent marsh species.

Future efforts could build on the simple approach used in this study to determine areas in the upper (higher) and lower portions of the irregularly flooded wetland zone by using techniques like those used by Holmquist and Windham-Meyers (2022) to estimate the general zonation within the irregularly flooded wetland zone while also incorporating elevation uncertainty. Finally, future efforts could explore how the framework could be enhanced by using synthetic aperture radar, which can delineate flooded vegetation (Rangoonwala et al., 2016), detecting inundation with optical imagery (O'Connell et al., 2017; Narron et al., 2022), and fusion with optical imagery for developing refined wetland masks (Lamb et al., 2019). In addition to updating the analysis along the northern Gulf of Mexico coast, future studies could expand this framework to the conterminous United States and beyond.

5. Conclusion

We used Monte Carlo simulations to incorporate elevation uncertainty and lidar-derived DEMs to create a probabilistic map of irregularly flooded wetlands. This product is the first regional map of elevation-based irregularly flooded wetland probability across the northern Gulf of Mexico coast. Our approach integrated findings from an updated literature review of coastal wetland elevation error and the use of spatial autocorrelation of coastal wetland elevation for random error field development. We found there was a significant, positive correlation when comparing the probability estimated from the DEM with the probability estimated from in situ elevation observations. Our results showed that DEM-based probability tended to be slightly lower than those estimated with in situ elevation observations. We found around the majority of the coastal wetland mask was included in either one of the classes that were unlikely to be irregularly flooded wetlands. Generally, these areas were split evenly between areas that were unlikely and low and unlikely and high. Most of the area classified as unlikely and low was in Louisiana and much of the area classified as unlikely and high was in the Everglades. The relative coverage of area classified as likely to be irregularly flooded wetlands covered around 13%, with the greatest coverage in south Florida, south Louisiana, and Texas. Regarding acquisition year and quality level, we found that older lidar data and lidar with a lower quality level seemed to have lower agreement between the probabilistic estimates from lidar data and in situ elevation observations. Most of the validation data were from emergent marsh, which tended to have a lower magnitude of error compared to woody wetlands, but a lower correlation coefficient. Future efforts could include updating the product produced in this study as new lidar data becomes available. Future updates could explore enhancing validation by using vegetation information and increasing the spread of points more evenly across the irregularly flooded wetland zone and for other wetland types, expanding to other areas, and predicting future irregularly flooded wetlands. The products developed from this study can serve many important applications including providing a baseline for gauging future wetland change with climate change and designing wetland vegetation and faunal monitoring programs (e.g., above-ground biomass transects and developing marsh bird surveys).

Author Responsibilities

NME and KOE designed the research. DBG, MSW and AMVF provided review and feedback of study methods. WCC, HRT, and NME performed the data analysis. JLP, JMS, and SCM all provided validation data for this study. NME drafted the manuscript, and all authors contributed to the manuscript editing and revision.

Declaration of Competing Interest

The authors declare that they have no known competing financial interests or personal relationships that could have appeared to influence the work reported in this paper.

Acknowledgments

This paper is a result of research funded by the National Oceanic and Atmospheric Administration's RESTORE Science Program under award NA19NOS4510195 to Mississippi State University and the USGS. We thank many individuals for providing feedback on draft products or assisting with in situ elevation data product availability, including Karrie Arnold, Eric Brunden, Kevin Buffington, Chris Butler, Jeremy Conrad, Jim Cox, Warren Conway, Mark Danaher, Christopher Gabler, Rebecca Howard, Brita Jessen, Erik Johnson, Kevin Kalasz, Peter Kappes, Joseph Lancaster, Heather Levy, Jonathon Lueck, Jonathan Moczygemba, Jena Moon, Michael Osland, Maulik Patel, Colt Sanspree, Amy Schwarzer, Fred Sklar, Eric Soehren, Camille Stagg, Karen Thorne, Will Underwood, William Vermillion, Jenneke Visser, Barry Wilson, Jennifer Wilson, Bernard Wood, and Woody Woodrow. We thank Neil Ganju from the USGS Woods Hole Coastal and Marine Science Center and three anonymous peer reviewers for their feedback on this work. Any use of trade, firm, or product names is for descriptive purposes only and does not imply endorsement by the U. S. Government.

References

Alizad, K., Medeiros, S.C., Foster-Martinez, M.R., Hagen, S.C., 2020. Model Sensitivity to Topographic Uncertainty in Meso- and Microtidal Marshes. IEEE J. Sel. Top. Appl. Earth Obs. Remote Sens. 13, 807–814. https://doi.org/10.1109/JSTARS.2020.2973490.

Anderson, C.P., Carter, G.A., Waldron, M.C.B. 2022. Precise Elevation Thresholds Associated with Salt Marsh–Upland Ecotones along the Mississippi Gulf Coast. Ann. Am. Assoc. Geogr. 112(7), 1850–1865. https://doi.org/10.1080/24694452.2022.2047593.

Andrews, B.M. 2022, The effects of short-term sea level rise on vegetation communities in coastal Mississippi. Theses and Dissertations 5407. https://scholarsjunction.msstate.edu/td/5407.

Anselin, L., Ibnu Syabri, I., Kho, Y., 2006. GeoDa: An Introduction to Spatial Data Analysis. Geogr. Anal. 38(1), 5–22. https://doi.org/10.1111/j.0016-7363.2005.00671.x.

ASPRS, 2015. ASPRS positional accuracy standards for digital geospatial data. Photogramm. Eng. Remote Sens. 81, A1–A26. https://doi.org/10.14358/PERS.81.3.A1-A26.

Barbier, E.B., Hacker, S.D., Kennedy, C., Koch, E.W., Stier, A.C., Silliman, B.R., 2011. The value of estuarine and coastal ecosystem services. Ecol. Monogr. 81, 169–193. https://doi.org/10.1890/10-1510.1.

Brophy, L.S., Greene, C.M., Hare, V.C., Holycross, B., Lanier, A., Heady, W.N., O'Connor, K., Imaki, H., Haddad, T., Dana, R., 2019. Insights into estuary habitat loss in the western United States using a new method for mapping maximum extent of tidal wetlands. PLoS ONE 14(8), e0218558. https://doi.org/10.1371/journal.pone.0218558.

Brown, J.F., Tollerud, H.J., Barber, C.P., Zhou, Q., Dwyer, J.L., Vogelmann, J.E., Loveland, T.R., Woodcock, C.E., Stehman, S.V., Zhu, Z., Pengra, B.W., Smith, K., Horton, J.A., Xian, G., Auch, R.F., Sohl, T.L., Sayler, K.L., Gallant, A.L., Zelenak, D., Reker, R.R., Rover, J., 2020. Lessons learned implementing an operational continuous United States national land change monitoring capability: The Land Change Monitoring, Assessment, and Projection (LCMAP) approach. Remote Sens. Environ. 238, 111356. https://doi.org/10.1016/j.rse.2019.111356.

Brunden, E., Underwood, W., Arnold, K., in review, Coastal wetland elevation survey of Weeks Bay National Estuarine Research Reserve, Alabama, 2016–2018 [dataset]. U.S. Geological Survey data release. https://doi.org./10.5066/P9Q2592L.

Buffington, K.J., Dugger, B.D., Thorne, K.M., Takekawa, J.Y., 2016. Statistical correction of lidar-derived digital elevation models with multispectral airborne imagery in tidal marshes. Remote Sens. Environ. 186, 616–625. http://dx.doi.org/10.1016/j.rse.2016.09.020.

Buffington, K.J., Thorne, K.M., 2022. Elevation survey across southwest Florida coastal wetlands, 2021 [dataset]. U.S. Geological Survey data release. https://doi.org/10.5066/P9POUPH5.

Byrd, K.B., Ballanti, L., Thomas, N., Nguyen, D., Holmquist, J.R., Simard, M., Windham-Myers, L., 2018. A remote sensing-based model of tidal marsh aboveground carbon stocks for the conterminous United States. ISPRS J. Photogramm. Remote Sens. 139, 255–271. https://doi.org/10.1016/j.isprsjprs.2018.03.019.

Cooper, H.M., Fletcher, C.H., Chen, Q., Barbee, M.M., 2013. Sea-level rise vulnerability mapping for adaptation decisions using lidar DEMs. Prog. Phys. Geogr. 37, 745–766. https://doi.org/10.1177/0309133313496835.

Cooper, H.M., Zhang, C., Davis, S.E., Troxler, T.G., 2019. Object-based correction of LiDAR DEMs using RTK-GPS data and machine learning modeling in the coastal Everglades. Environ. Model. Softw. 112, 179–191. https://doi.org/10.1016/j.envsoft.2018.11.003.

Cowardin, L.M., Carter, V., Golet, F.C., LaRoe, E.T., 1979. Classification of Wetlands and Deepwater Habitats of the United States. FWS/OBS-79/31. https://www.fws.gov/wetlands/Documents/Classification-of-Wetlands-and-Deepwater-Habitats-of-the-United-States.pdf.

Dale, L.L., Chivoiu, B., Osland, M.J., Enwright, N.M., Thorne, K.M., Guntenspergen, G.R., and Grace, J.B., 2022. Estuarine drainage area boundaries for the conterminous United States [dataset], U.S. Geological Survey data release. https://doi.org/10.5066/P9LPN3YY.

Enwright, N.M., Cheney, W.C., Evans, K., Thurman, H.R., Woodrey, M.S., Fournier, A.M.V., Bauer, A., Cox, J., Goehring, S., Hill, H., Hondrick, K., Kappes, P., Levy, H., Moon, J., Nyman, J.A., Pitchford, J., Storey, D., Sukiennik, M., and Wilson, J., 2022. Mapping irregularly flooded wetlands, high marsh, and salt pannes/flats along the northern Gulf of Mexico coast [dataset]. U.S. Geological Survey data release, https://doi.org/10.5066/P9MLO26U.

Enwright, N.M., Hartley, S.B., Couvillion, B.R., Brasher, M.G., Visser, J.M., Mitchell, M.K., Ballard, B.M., Parr, M.W., Wilson, B.C., 2015. Delineation of marsh types from Corpus Christi Bay, Texas, to

Perdido Bay, Alabama, in 2010. U.S. Geological Survey Scientific Investigations Map 3336. http://dx.doi.org/10.3133/sim3336.

Enwright, N.M., Wang, L., Borchert, S.M., Day, R.H., Feher, L.C., Osland, M.J., 2018. The Impact of Lidar Elevation Uncertainty on Mapping Intertidal Habitats on Barrier Islands. Remote Sens. 10, 5. https://doi.org/10.3390/rs10010005.

Gabler, C.A., Osland, M.J., Grace, J.B., Stagg, C.L., Day, R.H., Hartley, S.B., Enwright, N.M., From, A.S., McCoy, M.L., McLeod, J.L., 2017. Macroclimatic change expected to transform coastal wetland ecosystems this century. Nat. Clim. Chang. 7, 142–147. https://doi.org/10.1038/nclimate3203.

Ganju, N.K., Couvillion, B.R., Defne, Z., Ackerman, K.V., 2022. Development and Application of Landsat‐Based Wetland Vegetation Cover and UnVegetated‐Vegetated Marsh Ratio (UVVR) for the Conterminous United States. Estuaries Coast. 45, 1861–1878. https://doi.org/10.1007/s12237-022-01081-x.

Gesch, D.B., 2018. Best Practices for Elevation-Based Assessments of Sea-Level Rise and Coastal Flooding Exposure. Front. Earth Sci. 6. https://doi.org/10.3389/feart.2018.00230.

Gesch, D.B., Oimoen, M.J., Evans, G.A., 2014. Accuracy Assessment of the U.S. Geological Survey National Elevation Dataset, and Comparison with Other Large-Area Elevation Datasets—SRTM and ASTER. U.S. Geological Survey Open-File Report 2014–1008. https://dx.doi.org/10.3133/ofr20141008.

Greenberg, R., Maldonado, J.E., Droege, S., McDonald, M.V., 2006. Tidal marshes: A global perspective on the evolution and conservation of their terrestrial vertebrates. Bioscience 56(8), 675–685. https://doi.org/10.1641/0006-3568(2006)56[675:TMAGPO]2.0.CO;2.

Holmquist, J.R., Windham-Myers, L., 2022. A Conterminous USA-Scale Map of Relative Tidal Marsh Elevation. Estuaries Coast. 45, 1596–1614. https://doi.org/10.1007/s12237-021-01027-9.

Holmquist, J.R., Windham-Myers, L., Bernal, B., Byrd, K.B., Crooks, S., Gonneea, M.E., Herold, N., Knox, S.H., Kroeger, K.D., McCombs, J., Megonigal, J.P., Lu, M., Morris, J.T., Sutten-Grier, A.E., Troxler, T.G., Weller, D.E., 2018. Uncertainty in United States coastal wetland greenhouse gas inventorying. Environ. Res. Lett. 13, 115005. https://doi.org/10.1088/1748-9326/aae157.

IPCC, 2022. Climate Change 2022: Mitigation of Climate Change. Contribution of Working Group III to the Sixth Assessment Report of the Intergovernmental Panel on Climate Change. Cambridge University Press, Cambridge, UK and New York, NY, USA. https://doi.org/10.1017/9781009157926.

Jennerjahn, T.C., Gilman, E., Krauss, K.W., Lacerda, L.D., Wolanski, E., 2017. Mangrove ecosystems under climate change. In: Riveria-Monroy, V.H., Lee, S.Y., Kristensen, E., Twilley, R.R. (Eds.), Mangrove ecosystems: a global biogeographic perspective. Springer, pp. 211-244. https://doi.org/10.1007/978-3-319-62206-4_7.

Kidwell, D.M., Dietrich, J.C., Hagen, S.C., Medeiros, S.C., 2017. An earth's future special collection: Impacts of the coastal dynamics of sea level rise on low-gradient coastal landscapes. Earth's Future 5, 2–9. https://doi.org/10.1002/2016EF000493.

Knutson, T.R., McBride, J.L., Chan, J., Emanuel, K., Holland, G., Landsea, C., Held, I., Kossin, J.P., Srivastava, A.K., Sugi, M., 2010. Tropical cyclones and climate change. Nat. Geosci. 3(3), 157–163. https://doi.org/10.1038/ngeo779.

Koma, Z., Zlinsky, A., Bekő, L., Burai, P., Seijmonsbergen, S.C., Kissling, W.D., 2021. Quantifying 3D vegetation structure in wetlands using differently measured airborne laser scanning data. Ecol. Indic. 127, 107752. https://doi.org/10.1016/j.ecolind.2021.107752.

Kulp S.A., Strauss, B.H., 2019. New elevation data triple estimates of global vulnerability to sea-level rise and coastal flooding. Nat. Commun. 10, 4844. https://doi.org/10.1038/s41467-019-12808-z.

Lamb, B.T., Tzortziou, M.A., McDonald, K.C., 2019. Evaluation of Approaches for Mapping Tidal Wetlands of the Chesapeake and Delaware Bays. Remote Sens. 11(20), 2366. https://doi.org/10.3390/rs11202366.

Liu H., Wang, L., Sherman, D., Gao, Y., and Wu Q., 2010. An object-based conceptual framework and computational method for representing and analyzing coastal morphological changes. Int. J. Geogr. Inf. Sci. 24(7), 1015-1041. https://doi.org/10.1080/13658810903270569.

Medeiros, S.C., Bobinsky, J.S., Abdelwahab, K., 2022. Locality of Topographic Ground Truth Data for Salt Marsh Lidar DEM Elevation Bias Mitigation. IEEE J. Sel. Top. Appl. Earth Obs. Remote Sens. 15, 5766–5775. https://doi.org/10.1109/JSTARS.2022.3189226.

Medeiros, S., Hagen, S., Weishampel, J., Angelo, J., 2015. Adjusting Lidar-Derived Digital Terrain Models in Coastal Marshes Based on Estimated Aboveground Biomass Density. Remote Sens. 7(4), 3507–3525. https://doi.org/10.3390/rs70403507.

Moon, J.A., Feher, L.C., Lane, T.C., Vervaeke, W.C., Osland, M.J., Head, D.M., Chivoiu, B.C., Stewart, D.R., Johnson, D.J., Grace, J.B., Metzer, K.L., Rankin, N.M., 2022. Surface Elevation Change Dynamics in Coastal Marshes Along the Northwestern Gulf of Mexico: Anticipating Effects of Rising Sea-Level and Intensifying Hurricanes. Wetlands 42, 49. https://doi.org/10.1007/s13157-022-01565-3.

Moon, J.A., Lehnen, S.E., Metzger, K.L., Squires, M.A., Brasher, M.G., Wilson, B.C., Conway, W.C., Haukos, D.A., Davis, B.E., Rohwer, F.C., Wehland, E.M., Ballard, B.M. 2021. Projected impact of sea-level rise and urbanization on mottled duck (*Anas fulvigula*) habitat along the Gulf Coast of Louisiana and Texas through 2100. Ecol. Indic. 132, 108276. https://doi.org/10.1016/j.ecolind.2021.108276.

Narron, C.R., O'Connell, Mishra, D.R., Cotton, D.L., Hawman, P.A., Mao, L., 2022. Flooding in Landsat across tidal systems (FLATS): An index for intermittent tidal filtering and frequency detection in salt marsh environments. Ecol. Indic. 141, 109045. https://doi.org/10.1016/j.ecolind.2022.109045.

NOAA, 2016, NOAA's Coastal Change Analysis Program (C-CAP) 2016 Regional Land Cover Change Data – Coastal United States [dataset]. NOAA. https://coast.noaa.gov/htdata/raster1/landcover/bulkdownload/30m_lc/CCAP_Parent_2016.xml.

NOAA, 2019a, 2015-2017 C-CAP Derived 10 meter Land Cover – BETA [dataset]. NOAA. https://coast.noaa.gov/htdata/raster1/landcover/bulkdownload/Beta/10m_LC/2015_2017_ccap_10m_beta.xml.

NOAA, 2019b, NOAA/NOS's VDatum: Vertical Datum Transformation. https://vdatum.noaa.gov/welcome.html. (accessed 5 September 2019).

NOAA, 2019c, Tide Tables 2020: East Coast of North and South America. https://tidesandcurrents.noaa.gov/tidetables/2020/ectt_2020_full_book.pdf (accessed 21 September 2022).

O'Connell, J.L., Mishra, D.R., Cotton, D.L., Wang, L., Alber, M., 2017. The Tidal Marsh Inundation Index (TMII): An inundation filter to flag flooded pixels and improve MODIS tidal marsh vegetation time-series analysis. Remote Sens. Environ. 201, 34–46. https://doi.org/10.1016/j.rse.2017.08.008.

Osland, M.J., Chivoiu, B., Enwright, N.M., Thorne, K.M., Guntenspergen G.R., Grace, J.B., Dale, L.L., Brooks, W., Herold, N., Day, J.W., Sklar, F.H., Swarzenski, C.M., 2022. Migration and transformation of coastal wetlands in response to rising seas. Sci. Adv. 8(26), eabo5174. https://doi.org/10.1126/sciadv.abo5174.

Osland, M.J., Enwright, N., and Stagg, C.L., 2013. Freshwater availability and coastal wetland foundation species: ecological transitions along a rainfall gradient. Ecology 95(10), 2789–2802. https://doi.org/10.1890/13-1269.1.

Rangoonwala, A., Enwright, N.M., Ramsey III, E., Spruce, J.P., 2016. Radar and optical mapping of surge persistence and marsh dieback along the New Jersey Mid-Atlantic coast after Hurricane Sandy. Int. J. Remote Sens. 37, 1692–1713. https://doi.org/10.1080/01431161.2016.1163748.

Reyer, A.J., Holland, C.L., Field, D.W., Cassells, J.E., and Alexander, C.E., 1988. The Distribution and Areal Extent of Coastal Wetlands in Estuaries of the Gulf of Mexico. National Oceanic and Atmospheric Administration.

Saintilan, N., Kovalenko, K.E., Guntenspergen, G., Rogers, K., Lynch, J.C., Cahoon, D.R., Lovelock, C.E., Friess, D.A., Ashe, E., Krauss, K.W., Cormier, N., Spencer, T., Adams, J., Raw, J., Ibanez, C.,

Scarton, F., Temmerman, S., Meire, P., Maris, T., Thorne, K., Brazner, J., Chmura, G.L., Bowron, T., Gamage, V.P., Cressman, K., Endris, C., Marconi, C., Marcum, P., Laurent. K.S., Reay, W., Raposa, K.B., Garwood, J.A., Khan, N., 2022. Constraints on the adjustment of tidal marshes to accelerating sea level rise. Science 377(6605), 526-527, https://doi.org/ 10.1126/science.abo7872.

Schmid, K.A., Hadley, B.C., Wijekoon, N., 2011. Vertical Accuracy and Use of Topographic LIDAR Data in Coastal Marshes. J. Coast. Res. 27(6A), 116–132. https://doi.org/10.2112/JCOASTRES-D-10-00188.1.

Sharp, L.A., Villani, R., McGinnis, T.E., Piazza, S.C., 2021. Louisiana's Coastwide Reference Monitoring System (CRMS) elevation data [dataset]. U.S Geological Survey data release. https://doi.org/10.5066/P97X3UL6.

Stagg, C.L., Osland, M.J., Moon, J.A., Feher, L.C., Laurenzano, C., Lane, T.C., Jones, W.R., Hartley, S.B., 2021. Extreme Precipitation and Flooding Contribute to Sudden Vegetation Dieback in a Coastal Salt Marsh. Plants 10, 1841. https://doi.org/10.3390/plants10091841.

Stagg, C.L., Osland, M.J., Moon, J.A., Hall, C.T., Feher, L.C., Jones, W.R., Couvillion, B.R., Hartley, S.B., and Vervaeke, W.C., 2020. Quantifying hydrologic controls on local- and landscape-scale indicators of coastal wetland loss. Ann. Bot. 125(2), 365–376. https://doi.org/10.1093/aob/mcz144.

Stoker, J.M., Abdullah, Q.A., Nayegandhi, A., Winehouse, J., 2016. Evaluation of single photon and geiger mode lidar for the 3D Elevation Program. Remote Sens. 8, 767. https://doi.org/10.3390/rs8090767.

Stoker J., Miller, B., 2022. The Accuracy and Consistency of 3D Elevation Program Data: A Systematic Analysis. Remote Sens. 14(4), 940. https://doi.org/10.3390/rs14040940.

Stout, J.P., 1984. Ecology of irregularly flooded salt marshes of the northeastern Gulf of Mexico: a community profile. FWS/OBS-85.

Su, J., Bork E., 2006. Influence of Vegetation, Slope, and LiDAR Sampling Angle on DEM Accuracy. Photogramm. Eng. Remote Sensing 72, 1265–1274. https://doi.org/10.14358/PERS.72.11.1265.

Sweet, W.V., Dusek, G., Obeysekera, J., Marra, J.J., 2018. Patterns and Projections of High Tide Flooding Along the U.S. Coastline Using a Common Impact Threshold. NOAA Technical Report NOS CO-OPS 086. https://tidesandcurrents.noaa.gov/publications/techrpt86_PaP_of_HTFlooding.pdf.

Tang, L., Myers, E., Shi, L., Hess, K., Carisio, A., Michalski, M., White, S., Hoang, C., 2018. Tidal Datums with Spatially Varying Uncertainty in North-East Gulf of Mexico for VDatum Application. J. Mar. Sci. Eng. 6(4), 114. https://doi.org/10.3390/jmse6040114.

Thompson, P.R., Widlansky M.J., Hamlington, B.D., Merrifield, M.A., Marra, J.J., Mitchum, G.T., Sweet, W., 2021. Rapid increases and extreme months in projections of United States high-tide flooding. Nat. Clim. Chang. 11, 584–590. https://doi.org/10.1038/s41558-021-01077-8.

Thorne, K.M., MacDonald, G.M., Ambrose, R.F., Buffington, K.J., Freeman, C.M., Janousek, C.N., Brown, L.N., Holmquist, J.R., Guntenspergen, G.R., Powelson, K.W., Barnard, P.L., Takekawa, J.Y., 2016. Effects of climate change on tidal marshes along a latitudinal gradient in California: U.S. Geological Survey Open-File Report 2016-1125. http://dx.doi.org/10.3133/ofr20161125.

Tolliver, J.D., Moore, A.M., Green, M.C., and Weckerly, F.W., 2018. Coastal Texas Black Rail Population States and Survey Effort. J. Wildl. Manage. 83(2), 312-324. https://doi.org/10.1002/jwmg.21589.

U.S. Fish and Wildlife Service, 2022. USFWS National Wetlands Inventory [dataset]. https://www.fws.gov/wetlands.

USGS, 2020. 1/3rd arc-second Digital Elevation Models (DEMs) - USGS National Map 3DEP Downloadable Data Collection [dataset]. https://nationalmap.gov/3DEP/.

USGS, 2022. Lidar Base Specification 2022 rev. A. https://www.usgs.gov/ngp-standards-and-specifications/lidar-base-specification-revision-history#2022revA (accessed 10 June 2022).

USNVC, 2022a. United States National Vegetation Classification Database 2.0.4 - G121 *Spartina patens* - *Iva frutescens* High Salt Marsh Group. Federal Geographic Data Committee, Vegetation Subcommittee. https://www1.usgs.gov/csas/nvcs/unitDetails/837345 (accessed 8 July 2022).

USNVC, 2022b. United States National Vegetation Classification Database 2.0.4 - G123 *Salicornia* spp. - *Sarcocornia* spp. - *Spartina spartinae* Tidal Flat & Panne Group. Federal Geographic Data Committee, Vegetation Subcommittee. https://www1.usgs.gov/csas/nvcs/unitDetails/837392 (accessed 8 July 2022).

Wechsler, S.P., Kroll, C.N., 2006. Quantifying DEM uncertainty and its effect on topographic parameters. Photogramm. Eng. Remote Sens. 72, 1081–1090. https://doi.org/10.1007/978-94-011-0427-2_13.

Zervas, C.E., 2013. Extreme Water Levels of the United States. NOAA Technical Report NOS CO-OPS 067.

Zhao, Q., Bai, J., Huang, L., Gu, B., Lu, Q., Gao, Z. 2016. A review of methodologies and success indicators for coastal wetland restoration. Ecol. Indic. 60, 442–452. https://doi.org/10.1016/j.ecolind.2015.07.003.

Appendix A

1. Supplemental methods

1.1. Coastal wetland mask

The coastal wetland mask also included adjacent wetlands that were connected to estuarine wetlands using 8-pixel connectivity (i.e., connectivity that can occur through cells in both cardinal and diagonal directions). Based on visual inspection, we also added palustrine emergent marsh and unconsolidated shore wetlands that were within 3 pixels of connected estuarine and adjacent palustrine wetlands. These steps were completed for both datasets and then combined to determine the maximum extent of both masks. The final mask included water by using morphological operations to expand a mask by 3 pixels, which was used to include water areas from the both of the 2016 National Oceanic and Atmospheric Administration's Coastal Change assessment land cover datasets (i.e., 30-m 2016 land cover dataset and the 10-m 2016 BETA land cover dataset).

1.2. Elevation data processing

For each DEM, we determined the value assigned to hydroflattened areas and set these pixels to "No Data." Next, we resampled the DEMs from their native resolution to a 10-m DEM using the aggregate tool in Esri ArcGIS Pro. During this process, the minimum elevation of the 1-m DEM cells that fell within the new 10-m DEM cells was set as the elevation value. The rationale for resampling the DEM instead of simply using the standard 1/3 arc-second seamless product was that a moderate-resolution DEM would increase computation efficiency for the expansive spatial extent of this study and assigning the minimum value for the resampled DEM could help reduce potential elevation error (Schmid et al.,

2011). We used NOAA's VDatum v4.0 (NOAA, 2019) to transform the vertical datum of the DEMs at a spatial resolution of 10 m from the NAVD88. Similar to the process used by Defne et al. (2020), we extrapolated transformation values to inland areas by using inverse distance weighted interpolation.

1.3. Literature review to derive estimates of coastal wetland elevation error

We conducted a literature review to derive estimates of coastal wetland elevation error in lidar data. For this review, we documented the pulse spacing, elevation error, ground truth source, and study location. If available, we documented the 95th percentile of the error, which is the recommended metric by the ASPRS for vertical error for areas that include vegetated areas (ASPRS, 2015), due to a typical non-normal error distribution in vegetated areas. In other cases, the mean and standard deviation or, if reported, the RMSE, were documented. For results reported as the mean and standard deviation of error, the linear error at 95% confidence was estimated by multiplying the standard deviation by 1.96 and adding it to the mean. Likewise, in cases with a RMSE, we assumed normality and converted the RMSE value to an estimate of the 95th percentile of the error by multiplying the RMSE by 1.96. We took the maximum value for studies that reported error values by plant species. Additionally, we removed outliers, which were defined as values that were greater than 1.5 times the interquartile range. Finally, the mean value of the 95th percentile/confidence error estimates was calculated. The final wetland elevation error estimate was calculated by dividing the mean value without outliers by 2 (i.e., similar to 1.96). To be conservative, we truncated the wetland elevation error estimate to cm precision (i.e., 0.23 m) and then multiplied by 1,000 (i.e., 230).

1.4. Spatial autocorrelation of coastal wetland elevation

By watershed, we masked the DEMs to the coastal wetland mask. To avoid boundary issues, we buffered each watershed by 5 km. To increase computational efficiency, we resampled the DEMs from 10 to 100 m using bilinear interpolation. Next, these data were converted to point shapefiles. The spatial

autocorrelation analysis used all point pairs for this assessment except for four watersheds, which used a 50% random sample due to computational limitations. The median distance for zero spatial autocorrelation was calculated by region and the value was rounded to the nearest km (Table S1). We analyzed Mobile Bay as a stand-alone watershed and included Ten Thousand Islands with the West Peninsula Florida region for spatial autocorrelation, but we grouped this watershed with the Everglades region for reporting.

Table S1. Coastal wetland elevation distance for zero spatial autocorrelation by watershed and region along the northern Gulf of Mexico, USA. The median zero spatial autocorrelation distance for each region was rounded to the nearest km. See Figure 1 for regional and watershed boundaries.

Region	Watershed	Zero spatial autocorrelation distance (m)	Median zero spatial autocorrelation distance (m)
Laguna Madre	Lower Laguna Madre	7,425	16,000
	Upper Laguna Madre	1,6320	
	Baffin Bay	19,355	
Texas Mid-Coast	Corpus Christi Bay	9,094	11,000
	Aransas Bay	13,932	
	San Antonio Bay	10,663	
	Matagorda Bay	17,185	
	Brazos River	5,934	
	Austin-Oyster	9,233	
	West Galveston Bay	11,965	
Chenier Plain	East Galveston Bay	16,700	18,000
	Sabine Lake	8,500	
	Calcasieu Lake	19,500	
	Mermentau River	35,220	
Mid-Deltaic Plain	Atchafalaya/Vermilion Bays	50,934	51,000
Deltaic Plain	Terrebonne/Timbalier Bays	26,078	28,000
	Barataria Bay	35,654	
	Mississippi River	22,004	
	Breton/Chandeleur Sound	28,964	
Mississippi Sound	Lake Borgne	9,223	9,000
	Lake Pontchartrain	9,574	10,000
	West Mississippi Sound	6,907	7,000
	East Mississippi Sound	6,220	6,000
Mississippi Sound — Mobile Bay	Mobile Bay	27,112	27,000
Florida Panhandle	Perdido Bay	3,912	5,000
	Pensacola Bay	3,843	
	Choctawhatchee Bay	5,528	
	St. Andrew Bay	12,345	
Florida Big Bend	Apalachicola Bay	21,240	5,000
	Apalachee Bay	29,960	
	Econfina-Steinhatchee	4,930	
	Suwannee River	3,880	
	Waccasassa	5,040	
	Withlacoochee	3,780	
	Crystal-Pithlachascotee	10,890	
West Peninsula Florida	Tampa Bay	10,574	10,000
	Sarasota Bay	9,227	
	Charlotte Harbor	8,167	
	Caloosahatchee River	14,222	

	Estero Bay	12,878	
	Rookery Bay	9,715	
	North Ten Thousand Islands	4,708	
Everglades	Everglades West Coast	39,868	53,000
	Everglades	66,233	
Florida Keys	Florida Bay-Florida Keys	18,780	19,000

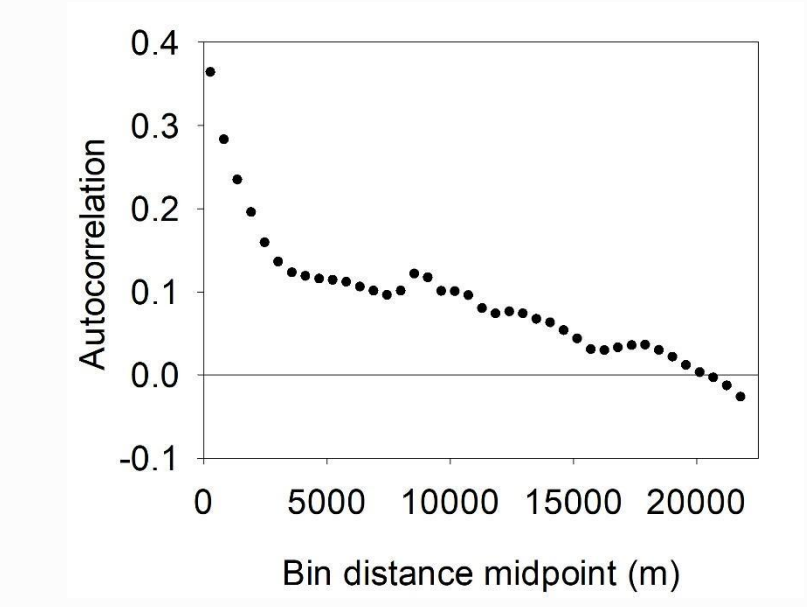

Figure S1. Example of spatial autocorrelation of coastal wetland elevation for Apalachicola, Florida (USA).

1.5. Monte Carlo simulations

To increase efficiency, the Monte Carlo analysis was conducted using numeric values of elevation and uncertainty as integer and not floating point. This meant that the DEMs and uncertainty estimates were multiplied by 1,000 and converted to integer (e.g., integer could include mm precision; a value of 157 would be equal to 0.157 m).

The upper bound included the cumulative error using regional uncertainty from VDatum for the mean higher high water (MHHW) datum and the high-tide flooding level, whereas the lower bound included the regional uncertainty from VDatum for the MHW datum. For uncertainty information by region see Table

S2. The cumulative vertical uncertainty (CVU) for the upper bound was calculated using a root sum of squares (Eq. 1) as recommended by Gesch (2018).

$$CVU = \sqrt{VTU^2 + FLU^2} \quad (1)$$

Where *VTU* is the vertical transformation uncertainty from VDatum for the MHHW datum and *FLU* is the uncertainty for the high-tide flooding level.

For each iteration, pixels in the DEM were coded as "1" if the elevation with uncertainty propagation fell within the irregularly flooded wetland zone (i.e., between MHW and NOAA's high-tide flooding level) and "0" if they fell outside the irregularly flooded wetland zone. The probability of a pixel being irregularly flooded was calculated by summing the binary simulation outputs and dividing by 1,000 (i.e., the number of iterations). The output files of the Monte Carlo simulations included non-wetland areas. We removed non-wetlands by restricting the probabilistic outputs to the coastal wetland mask.

Table S2. Regional elevation uncertainty information—in centimeters multiplied by 1,000—used for Monte Carlo simulations representing the upper and lower bound of the irregularly flooded wetland zone along the northern Gulf of Mexico, USA. Uncertainty sources are from the National Oceanic and Atmospheric Administration's (NOAA) flooding level (HTF; Sweet et al., 2018) and NOAA's VDatum 4.0 tool (NOAA, 2019). VDatum uncertainty estimates were truncated to convert the values to integers. See Figure 1 for regional and watershed boundaries. UB, upper bound; LB, lower bound.

		UB uncertainty			LB uncertainty
Region	**Watershed**	**HTF**	**VDatum**	**Cumulative**	**VDatum**
Laguna Madre	Lower Laguna Madre	250	147	290	146
	Upper Laguna Madre	250	147	290	146
	Baffin Bay	250	147	290	146
Texas Mid-Coast	Corpus Christi Bay	250	147	290	146
	Aransas Bay	250	147	290	146
	San Antonio Bay	250	110	273	108
	Matagorda Bay	250	110	273	108
	Brazos River	250	110	273	108
	Austin-Oyster	250	110	273	108
	West Galveston Bay	250	110	273	108
Chenier Plain	East Galveston Bay	190	110	220	108
	Sabine Lake	190	110	220	108
	Calcasieu Lake	190	108	219	108
	Mermentau River	190	108	219	108
Mid-Deltaic Plain	Atchafalaya/Vermilion Bays	190	160	249	160
Deltaic Plain	Terrebonne/Timbalier Bays	190	160	249	160
	Barataria Bay	190	160	249	160
	Mississippi River	190	160	249	160
	Breton/Chandeleur Sound	190	160	249	160
Mississippi Sound	Lake Borgne	190	160	249	160
	Lake Pontchartrain	190	160	249	160
	West Mississippi Sound	190	160	249	160
	East Mississippi Sound	190	160	249	160
	Mobile Bay	190	58	199	57
Florida Panhandle	Perdido Bay	190	58	199	58
	Pensacola Bay	190	58	199	58
	Choctawhatchee Bay	190	58	199	58
	St. Andrew Bay	190	54	198	54
Florida Big Bend	Apalachicola Bay	190	83	207	78
	Apalachee Bay	190	83	207	78
	Econfina-Steinhatchee	190	83	207	78
	Suwannee River	190	83	207	78
	Waccasassa	190	83	207	78
	Withlacoochee	190	83	207	78
	Crystal-Pithlachascotee	190	116	223	115
West Peninsula Florida	Tampa Bay	190	116	223	115
	Sarasota Bay	190	116	223	115

	Charlotte Harbor	190	116	223	115
	Caloosahatchee River	190	116	223	115
	Estero Bay	190	116	223	115
	Rookery Bay	190	58	199	58
Everglades	North Ten Thousand Islands	190	71	203	71
	Everglades West Coast	190	71	203	71
	Everglades	190	71	203	71
Florida Keys	Florida Bay-Florida Keys	190	58	199	58

1.6. Probabilistic output validation

A 2.5-m buffer was applied to all points. If a point was within 2.5 m of another point, then the maximum point was retained and the other point was omitted. The probability of the in situ points being irregularly flooded wetlands was estimated using a Monte Carlo process following an approach similar to the process applied to the DEMs. This process included 1,000 iterations and included tidal datum transformation and uncertainty and high-tide flooding level uncertainty values but did not include coastal wetland elevation error adjustment.

2. Literature review of lidar error results

We found a total of 23 studies that included coastal wetland elevation error statistics. The studies used lidar that ranged from 2003 to 2017 (Table S3). The studies were mostly from the USA, with seven studies along the West coast, four studies along the northern Gulf of Mexico, and 10 studies along the East coast (one from Canada). Based solely on pulse spacing per m^2, the lidar data could be characterized as roughly equal parts of quality level 2 data ($\geq$ 2 points/m^2) and quality level 3 data ($\geq$ 0.5 points/m^2). Two studies listed the ground truth source as differential global positioning system (GPS); however, most of the studies listed the ground truth source as real-time kinematic GPS (RTK GPS). The 95th percentile error or linear error with a 95% confidence ranged from 0.13 m to 1.27 m. For all studies, the median error was 0.47 m with an interquartile range of 0.32. The observation of 1.27 m was considered an outlier since it was greater than 1.5 times the interquartile range. With the outlier removed, the mean value was 0.46 m.

Table S3. Coastal wetland lidar error summary from literature. For elevation error estimates, "*" indicates that a maximum value was taken. 95P, 95th percentile; RMSE, Root mean square error; LE95, linear error at 95% confidence; ME, mean error; SD, standard deviation; MAE, mean absolute error; GPS, global positioning system; RTK GPS, real-time kinematic global positioning system. For presentation, we rounded all error estimates to the nearest cm.

Year	Pulse spacing (pts/m^2)	Elevation error (m)	Type	Ground truth source	Location	Source
2015	6	0.42	95P	RTK GPS	Dauphin Island, AL	Enwright et al. (2018)
2007	4	0.65	RMSE	RTK GPS	Apalachicola, FL	Medeiros et al. (2015)
		1.27	LE95			
2003	4	0.07	ME	RTK GPS	Georgetown, SC	Montané and Torres (2006)
		0.08	SD			
		0.24	LE95			
2008–2010	1–9	0.51*	95P	RTK GPS	West Coast of United States	Buffington et al. (2016)
2009	9	0.32	95P	RTK GPS	Sapelo Island, GA	Hladik and Alber (2012)
2007	0.7	0.230	RMSE	Static GPS	Charleston, SC	Schmid et al. (2011)
		0.45	LE95			
2008	7	0.45*	MAE	RTK GPS	Oregon coast	Ewald (2013)
		0.12	SD			
		0.68	LE95			
2010	≥2	0.30	95P	RTK GPS	San Pablo Bay, CA	McClure et al. (2016)
2010	5	0.33	RMSE	RTK GPS	Cape Cod, MA	Rogers et al. (2018)
		0.65	LE95			
2008	2	0.27*	RMSE	RTK GPS	Everglades, FL	Cooper et al. (2019)
		0.53	LE95			
2003	0.2	0.07	RMSE	Post-processed GPS	North Inlet, SC	Morris et al. (2005)
		0.13	LE95			
2003	0.7	0.05	ME	RTK GPS	Maddieanna Island, SC	Chassereau et al. (2011)
		0.28	SD			
		0.60	LE95			
2013	2	0.29*	RMSE	RTK GPS	Huelva, Spain	Fernandez-Nunez et al. (2017)
		0.57	LE95			
2011	1	0.15	ME	RTK GPS	Plum Island, MA	Alizad et al. (2020)
		0.05	SD			
		0.25	LE95			
2017	3.0	0.250	ME	RTK GPS	Fire Island, NY	Muñoz et al. (2019)
		0.16	SD			
		0.56	LE95			
2003	2.3	0.12	RMSE	Total station	San Francisco, CA	Rosso et al. (2006)
		0.24	LE95			
2003	7.8	0.02	ME	Differential GPS	Venice, Italy	Wang et al. (2009)
		0.06	SD			
		0.15	LE95			
2006	1	0.32*	ME	Differential GPS	Bay of Fundy, Canada	Millard et al. (2013)
		0.08	SD			
		0.47	LE95			
2003	1.9	0.18*	RMSE	Total station	Santa Barbara, CA	Sadro et al. (2007)
		0.35	LE95			
2010	1	0.26	RMSE	RTK GPS	San Francisco, CA	Buffington and Thorne (2019)
		0.51	LE95			

2017	2.9	0.29 0.56	RMSE LE95	RTK GPS	Suisun marsh, CA	Buffington et al. (2019a)
2010/ 2017	1.4	0.13 0.25	RMSE LE95	RTK GPS	Chesapeake Bay, MD	Buffington et al. (2019b)
2007/ 2017	0.8	0.45 0.87	RMSE LE95	RTK GPS	Collier County, FL	Buffington and Thorne (2022)

Table S4. Areal coverage (sq km) irregularly flooded wetland probability by bin by watershed along the northern Gulf of Mexico, USA. See Figure 1 for regional and watershed boundaries. Unlikely and low, probability ≤ 0.33 and below mid-point between mean high water and the NOAA high-tide flooding level (Sweet et al., 2018); Unlikely and high, probability ≤ 0.33 and above mid-point between mean high water and the NOAA high-tide flooding level; Likely as not, probability > 0.33 and ≤ 0.66; Likely, probability > 0.66.

		Coverage irregularly flooded wetland probability (km^2)				
Region	**Watershed**	**Unlikely and low**	**Unlikely and high**	**As likely as not**	**Likely**	**Total**
Laguna Madre	Lower Laguna Madre	146.92	404.33	280.93	213.33	1,045.51
	Upper Laguna Madre	11.06	196.52	114.25	124.90	446.73
	Baffin Bay	7.33	125.78	29.98	31.17	194.27
Texas Mid-Coast	Corpus Christi Bay	26.60	87.64	35.87	18.11	168.21
	Aransas Bay	96.62	201.43	70.26	28.41	396.72
	San Antonio Bay	43.86	181.11	65.29	55.69	345.96
	Matagorda Bay	127.57	350.31	154.26	150.56	782.70
	Brazos River	29.29	33.08	27.70	28.41	118.48
	Austin-Oyster	17.45	24.52	15.45	10.32	67.74
	West Galveston Bay	94.72	275.06	115.37	93.67	578.82
Chenier Plain	East Galveston Bay	309.61	71.76	124.53	127.16	633.06
	Sabine Lake	816.65	74.30	117.68	74.97	1,083.59
	Calcasieu Lake	499.93	36.84	135.17	100.91	772.86
	Mermentau River	1,497.86	4.59	381.49	217.92	2,101.87
Mid-Deltaic Plain	Atchafalaya/Vermilion Bays	1,744.01	10.74	494.49	105.73	2,354.98
Deltaic Plain	Terrebonne/Timbalier Bays	677.76	6.10	98.45	20.63	802.95
	Barataria Bay	759.79	33.47	492.60	254.21	1,540.07
	Mississippi River	18.50	201.89	24.54	27.25	272.19
	Breton/Chandeleur Sound	723.61	9.59	144.42	52.87	930.49
Mississippi Sound	Lake Borgne	336.96	13.43	43.69	14.53	408.60
	Lake Pontchartrain	274.60	6.48	43.53	5.91	330.51
	West Mississippi Sound	83.39	13.22	20.77	11.76	129.15
	East Mississippi Sound	95.09	14.13	45.13	19.38	173.72
	Mobile Bay	25.44	27.03	28.57	46.62	127.67
Florida Panhandle	Perdido Bay	7.05	9.75	6.78	13.54	37.11
	Pensacola Bay	34.20	11.97	10.19	22.09	78.44
	Choctawhatchee Bay	6.49	6.96	5.93	8.70	28.08
	St. Andrew Bay	24.51	46.59	23.68	28.46	123.24
Florida Big Bend	Apalachicola Bay	44.07	22.15	30.91	47.77	144.89
	Apalachee Bay	174.32	12.60	33.50	28.65	249.07
	Econfina-Steinhatchee	53.17	1.41	16.24	23.51	94.34
	Suwannee River	12.66	0.47	5.14	7.05	25.32
	Waccasassa	118.99	4.24	26.92	18.27	168.42
	Withlacoochee	5.39	2.14	0.72	0.51	8.75
	Crystal-Pithlachascotee	106.98	6.62	42.77	69.40	225.77
West Peninsula Florida	Tampa Bay	28.95	13.79	29.17	30.22	102.14
	Sarasota Bay	9.25	6.11	8.34	6.69	30.40

	Charlotte Harbor	70.43	24.18	80.35	95.06	270.02
	Caloosahatchee River	0.02	0.00	0.05	0.02	0.10
	Estero Bay	27.58	5.90	25.97	12.51	71.95
	Rookery Bay	53.84	19.51	22.61	16.94	112.90
Everglades	North Ten Thousand Islands	203.78	0.89	44.27	28.48	277.42
	Everglades West Coast	183.30	1,747.26	84.81	164.29	2,179.65
	Everglades	671.05	4,671.87	465.38	911.69	6,719.99
Florida Keys	Florida Bay-Florida Keys	55.22	7.17	48.20	42.78	153.37

References

Alizad, K., Medeiros, S.C., Foster-Martinez, M.R., Hagen, S.C., 2020. Model Sensitivity to Topographic Uncertainty in Meso- and Microtidal Marshes. IEEE J. Sel. Top. Appl. Earth Obs. Remote Sens. 13, 807–814. https://doi.org/10.1109/JSTARS.2020.2973490.

ASPRS, 2015. ASPRS positional accuracy standards for digital geospatial data. Photogramm. Eng. Remote Sens. 81, A1–A26. https://doi.org/10.14358/PERS.81.3.A1-A26.

Buffington, K.J., Dugger, B.D., Thorne, K.M., Takekawa, J.Y., 2016. Statistical correction of lidar-derived digital elevation models with multispectral airborne imagery in tidal marshes. Remote Sens. Environ. 186, 616–625. http://dx.doi.org/10.1016/j.rse.2016.09.020.

Buffington, K.J., Thorne, K.M., 2019, LEAN-corrected San Francisco Bay digital elevation model, 2018 [dataset]. U.S. Geological Survey data release. https://doi.org/10.5066/P97J9GU8.

Buffington, K.J., Thorne, K.M., 2022. Elevation survey across southwest Florida coastal wetlands, 2021 [dataset]. U.S. Geological Survey data release. https://doi.org/10.5066/P9POUPH5.

Buffington, K.J., Thorne, K.M., Carr, J.A., Guntenspergen, G.R., 2019b. LEAN-Corrected Chesapeake Bay Digital Elevation Models, 2019 [dataset]. U.S. Geological Survey data release. https://doi.org/10.5066/P9NQZXU3.

Buffington, K.J., Thorne, K.M., Takekawa, J.Y., Chappell, S., Swift, T., Feldheim, C., Squellati, A., Mardock, D.K., 2019a. LEAN-Corrected DEM for Suisun Marsh [dataset]. U.S. Geological Survey data release. https://doi.org/10.5066/P97R4ES3.

Chassereau, J.E., Bell, J.M., Torres, R., 2011. A comparison of GPS and lidar salt marsh DEMs. Earth Surf. Process Landf. 36, 1770–1775. https://doi.org/10.1002/esp.2199.

Cooper, H.M., Zhang, C., Davis, S.E., Troxler, T.G., 2019. Object-based correction of LiDAR DEMs using RTK-GPS data and machine learning modeling in the coastal Everglades. Environ. Model. Softw. 112, 179–191. https://doi.org/10.1016/j.envsoft.2018.11.003.

Defne, Z., Aretxabaleta, A.L., Ganju, N.K., Kalra, T.S., Jones, D.K., Smith, K.E.L., 2020. A geospatially resolved wetland vulnerability index: Synthesis of physical drivers. PLoS ONE 15(1), e0228504. https://doi.org/10.1371/journal.pone.0228504.

Enwright, N.M., Wang, L., Borchert, S.M., Day, R.H., Feher, L.C., Osland, M.J., 2018. The Impact of Lidar Elevation Uncertainty on Mapping Intertidal Habitats on Barrier Islands. Remote Sens. 10, 5. https://doi.org/10.3390/rs10010005.

Ewald, M.J., 2013. Where's the ground surface? Elevation bias in LIDAR-derived digital elevation models due to dense vegetation in Oregon tidal marshes. https://ir.library.oregonstate.edu/concern/graduate_thesis_or_dissertations/2r36v250n.

Fernandez-Nunez, M., Burningham, H., Zújar, J.O., 2017. Improving accuracy of LiDAR-derived digital terrain models for saltmarsh management. J. Coast. Conserv. 21, 209–222. https://doi.org/10.1007/s11852-016-0492-2.

Gesch, D.B., 2018. Best Practices for Elevation-Based Assessments of Sea-Level Rise and Coastal Flooding Exposure. Front. Earth Sci. 6. https://doi.org/10.3389/feart.2018.00230.

Hladik, C., Alber, M., 2012. Accuracy assessment and correction of a LIDAR-derived salt marsh digital elevation model. Remote Sens. Environ. 121, 224–235. https://doi.org/10.1016/j.rse.2012.01.018.

McClure, A., Liu, X., Hines, E., Ferner, M.C., 2016., Evaluation of Error Reduction Techniques on a LIDAR-Derived Salt Marsh Digital Elevation Model. J. Coast. Res. 32(2), 424–433. https://doi.org/10.2112/JCOASTRES-D-14-00185.1.

Medeiros, S., Hagen, S., Weishampel, J., Angelo, J., 2015. Adjusting Lidar-Derived Digital Terrain Models in Coastal Marshes Based on Estimated Aboveground Biomass Density. Remote Sens. 7(4), 3507–3525. https://doi.org/10.3390/rs70403507.

Millard, K., Redden, A.M., Stewart, H., 2013. Use of GIS and high resolution LiDAR in salt marsh restoration site suitability assessments in the upper Bay of Fundy, Canada. Wetl. Ecol. Manag. 21, 243–262.

Montané, J.M., Torres, R., 2006. Accuracy Assessment of LIDAR Saltmarsh Topographic Data Using RTK GPS. Photogramm. Eng. Remote Sensing 72, 961–967. https://doi.org/10.14358/PERS.72.8.961.

Morris, J.T., Porter, D., Neet, M., Noble, P.A., Schmidt, L., Lapine, L.A., Jensen, J.R., 2005. Integrating LIDAR elevation data, multi‐spectral imagery and neural network modelling for marsh characterization. Int. J. Remote Sens. 26(23), 5221–5234. https://doi.org/10.1080/01431160500219018.

Muñoz, D.F., Cissell, J.R., Moftakhari, H., 2019. Adjusting Emergent Herbaceous Wetland Elevation with Object-Based Image Analysis, Random Forest and the 2016 NLCD. Remote Sens. 11(20), 2346. https://doi.org/10.3390/rs11202346.

NOAA, 2019, NOAA/NOS's VDatum: Vertical Datum Transformation. https://vdatum.noaa.gov/welcome.html. (accessed 5 September 2019).

Rogers, J.N., Parrish, C.E., Ward, L.G., Burdick, D.M., 2018. Improving salt marsh digital elevation model accuracy with full-waveform lidar and nonparametric predictive modeling. Estuar. Coast. Shelf Sci. 202, 193–211. https://doi.org/10.1016/j.ecss.2017.11.034.

Rosso, P.H., Ustin, S.L., Hastings, A., 2006. Use of lidar to study changes associated with *Spartina* invasion in San Francisco Bay marshes. Remote Sens. Environ. 100(3), 295–306.

Sadro, S., Gastil-Buhl, M., Melack, J., 2007. Characterizing patterns of plant distribution in a southern California salt marsh using remotely sensed topographic and hyperspectral data and local tidal fluctuations. Remote Sens. Environ. 110(2), 226–239. https://doi.org/10.1016/j.rse.2007.02.024.

Schmid, K.A., Hadley, B.C., Wijekoon, N., 2011. Vertical Accuracy and Use of Topographic LIDAR Data in Coastal Marshes. J. Coast. Res. 27(6A), 116–132. https://doi.org/10.2112/JCOASTRES-D-10-00188.1.

Sweet, W.V., Dusek, G., Obeysekera, J., Marra, J.J., 2018. Patterns and Projections of High Tide Flooding Along the U.S. Coastline Using a Common Impact Threshold. NOAA Technical Report NOS CO-OPS 086. https://tidesandcurrents.noaa.gov/publications/techrpt86_PaP_of_HTFlooding.pdf.

Wang, C., Menenti, M., Stoll, M-.P., Feola, A., Belluco, E., Marani M., 2009. Separation of Ground and Low Vegetation Signatures in LiDAR Measurements of Salt-Marsh Environments. IEEE J. Sel. Top. Appl. Earth Obs. Remote Sens. 47(7), 2014–2023. https://doi.org/10.1109/TGRS.2008.2010490.